ÉCOLE POLYTECHNIQUE
FÉDÉRALE DE LAUSANNE

Master thesis

Betatron squeeze optimisation at the Large Hadron Collider based on first year of operation data

Author :
X. Buffat

Under the supervision of :
Prof. L. Rivkin (EPFL)
Dr. S. Redaelli (CERN)

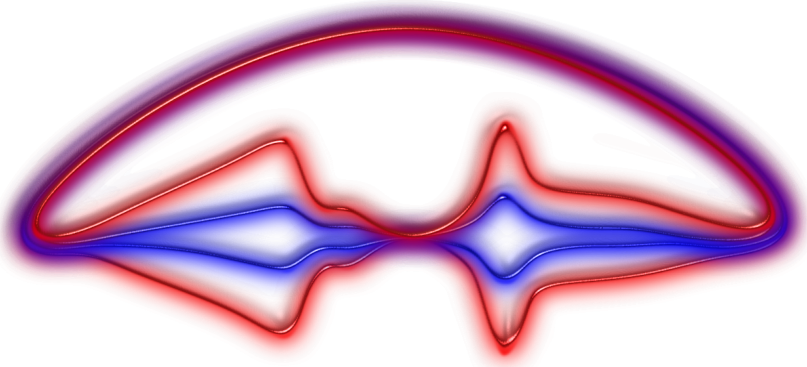

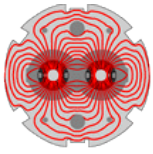

Lausanne, January 20, 2011

Contents

List of acronyms

ALICE	A Large Ion Collider Experiment
ATLAS	A Toroidal LHC Apparatus
BBQ	base band tune
BCT	beam current transformer
BLM	beam loss monitor
BP	beam process
BPM	beam position monitor
CCC	CERN Control Centre
CERN	European Laboratory for particle physics
CMS	Compact Muon Solenoid
FiDeL	Field Description for the LHC
IP	interaction point
IR	interaction region
LHC	Large Hadron Collider
LHCb	LHC beauty experiment
LSA	LHC software architecture
MADX	Methodical Accelerator Design X
MP	matched point
MS	matching section
OFB	orbit feedback system
PC	power converter
QFB	tune feedback system
QPS	quench protection system
RF	radio frequency
TOTEM	Total Elastic and diffractive cross section Measurement

Acknowledgements

Firstly, I would like to greatly thank Prof. L. Rivkin for giving me the opportunity to work at CERN on the Large Hadron Collider and for his constant support through the different administrative processes to get the appropriate positions, as well as for his advices concerning the work presented in this thesis. Secondly, the whole operation team of the Large Hadron Collider deserves to be thanked for welcoming me so nicely in their working environment. In particular, I would like to thank Dr. S. Redaelli for the numerous explanations, ideas and advices provided during our many discussions and for his help in the appreciation of my work among the team. I am also very thankful to his doctoral student, G. Müller whose help for the technical part, he made the painful job of getting started pretty easy and greatly improved my analysis power by introducing me to CERN's Java environment and by providing me important tools.

I would like to profit from the occasion to try to express my infinite thankfulness to my parents for their financial support, and most importantly for their indefatigable moral support, their love, throughout my studies and my life. I owe them everything that I have, everything that I am.

Chapter 1

Introduction

The Large Hadron Collider (LHC) is the world's largest hadron collider, which aims at pushing further our understanding of the universe by colliding protons and lead ions to probe the interaction between elementary particles at the TeV scale. The LHC has been designed to achieve high requirements to potentially reveal new physics, beyond the standard model of particle physics. There are two main requirements, first, high collision energy is needed, such that heavy particles may be produced and unknown high energy processes may occur. Secondly, the amount of collision produced, characterised by the luminosity of the collider, is the second most important requirement for high energy physics. Indeed, the description of the process undergone by the colliding high energy particles is essentially stochastic, therefore the measurements heavily rely on statistics. It is important to note that high energy processes are often shadowed by known processes that already occur at lower energy, as they have a much lower cross section, therefore a large amount of collision is needed in order to obtain precise statistics.
Four main experiments are installed around the LHC ring in order to detect particles resulting from the collision of high energy particles at distinct interaction points (IPs). A Toroidal LHC Apparatus (ATLAS)[1] at IP1 and the Compact Muon Solenoid (CMS)[2] at IP5 are two all purpose detectors, designed to detect the largest amount of particle with the highest precision. Their main purpose is the determination of the existence or non-existence of the Higgs boson. The LHC beauty experiment (LHCb)[3] at IP8 is optimized for the detection of event with beauty particles in order to study the CP symmetry breaking. A Large Ion Collider Experiment (ALICE)[4] at IP2 is optimized for heavy ion operation for quark-gluon plasma study. Whereas ATLAS and CMS are demanding the highest collision rate possible, in order to obtain a large statistics for the study of rare events, LHCb and ALICE demands on collision rates are lower.

Based on the experience acquired from the previous large accelerators, the commissioning of the LHC is done step by step towards the nominal performances. The main nominal parameters are shown in the table 1.1, as well as the configuration and achievements during 2010 operation with protons. Much remain to be done before reaching to the nominal performances. Among them, the minimum β^*, which is an important parameter for the collision rate, has not yet been reached, in particular at the high luminosity experiments. Indeed, the operation needed to reduce the β^*, the betatron squeeze, is a critical operation that needs to be performed properly, especially at low β^*. In particular, the experience of Tevatron at Fermilab emphasise the sensitivity of the machine during this phase. Indeed, after several years of operation, it is still is one of the most critical phase in the operation of the Tevatron. [5]
The decrease of energy proposed after the accident of 2008 increases the limitations in aperture, which motivated a limitation of β^* to 3.5m. This limitation has, however, allowed to quickly go through the

	nominal	2010 proton run
Energy [TeV]	7	3.5
Peak Luminosity [10^{34} cm^{-2} s^{-1}]	1	0.02
Maximum stored energy per beam [MJ]	362	28
Maximum number of bunch	2808	368
Bunch intensity [10^{11}p]	1.15	1.3
β^* at IP1 and IP5 [m]	0.55	2-3.5
β^* at IP2 [m]	10	2-3.5
β^* at IP8 [m]	1 to 50	2-3.5

Table 1.1: LHC nominal parameters and 2010 proton run achievements. β^* of 2m have been achieved but routine operation was done with 3.5m at all IPs.

commissioning of the squeeze, therefore quickly obtain significant collision rates and go on with the commissioning of many other systems. Thus, the beam intensities have been increased rapidly, allowing to surpass the objective fixed for 2010 in term of delivered luminosity to the experiments. Moreover, this method has allowed to collect a significant amount of data during each phase of the preparation of the machine for collision, including the betatron squeeze, offering the possibility to analyse the performances achieved and the issues encountered. The issues may be understood and dealt with before introducing higher intensity beams and lower β^* when the protection of the machine against damages from the beams become a more and more critical issue. Moreover, the understanding of the each features of the machine may lead to important improvements of the operation.

This thesis present the performances achieved during the 2010 proton run regarding the squeezing of the beam at the IPs. Numerical simulation of the beam properties are introduced and validated by comparison with measurement in order to facilitate the understanding of the observed features. The simulation and measurements serve as a basis for the introduction of a new strategy for next year.

Chapter 2

Basic accelerator and beam physics

2.1 Synchrotron

Synchrotrons are currently the most common type of particle accelerator for high energy physics, they allow one to achieve the highest luminosity at the highest energy for reasonable cost. A synchrotron is made of a vacuum pipe closed on itself, in which particles are steered on a constant orbit, known as the reference orbit, by means of dipole magnets. Particles are kept together around the orbit by higher order magnets and accelerated using high amplitude alternative electric field, provided by radio frequency (RF) cavities. The reference orbit is kept constant by properly increasing the strength of the dipole with the energy of the particles. In order to follow the reference orbit, particles must enter the synchrotron with an already non-null velocity, therefore the performance of the synchrotron is highly dependent on the performance of its injector. Circulating in a finite vacuum pipe, particles constituting the beam are subject to different process that can lead them astray and eventually cause them to deposit their energy in the surrounding material. The motivation for accelerator and beam physics is to fully understand the motion of charge particles circulating in a real machine and design adequate systems to control them.

2.2 Classical electrodynamics

For the scope of this thesis, the dynamics of the beam is well described by classical electrodynamics. Moreover, as we will consider dynamics in the transverse plane with respect to the velocity of the particle, relativistic effects do not have to be taken into account. However, complexity quickly arise from the treatment of the motion of a particle in non-linear fields. The standard way to approach this task is to use Hamiltonian formalism and study term by term the multipole decomposition of an arbitrary field [6]. Although very interesting, these studies will not be addressed here. Indeed, the amplitude of the effects expected from the fields component decreases with increasing order. We can therefore settle for a treatment of low order field in the frame of this thesis. Lorentz force and Newton dynamics are sufficient. Let us consider a particle of mass m and charge q at a position x in an electric and magnetic fields $\overrightarrow{E}$ and $\overrightarrow{B}$.

$$\overrightarrow{F} = \overrightarrow{E} + q\left(\dot{\overrightarrow{x}} \times \overrightarrow{B}\right) \tag{2.2.1}$$

$$\overrightarrow{F} = m\ddot{\overrightarrow{x}} \tag{2.2.2}$$

where $\dot{}$ represent the time derivative. For high energy accelerators, like the LHC, steering and focusing of the beam is insured by magnetic fields, the use of electric fields is restricted to smaller accelerator and will not be discussed here. Therefore, the transverse dynamics of a particle in an accelerator can be described with the following equation.

$$\ddot{x} = \frac{q}{m}\left(\dot{\overrightarrow{x}} \times \overrightarrow{B}\right) \tag{2.2.3}$$

Let us understand the motion of a particle in low order fields.

Motion in a transverse dipole field Consider a particle moving, through the following magnetic field described in a Cartesian coordinate system,

$$\overrightarrow{B} = B_z \cdot \hat{e}_z \tag{2.2.4}$$

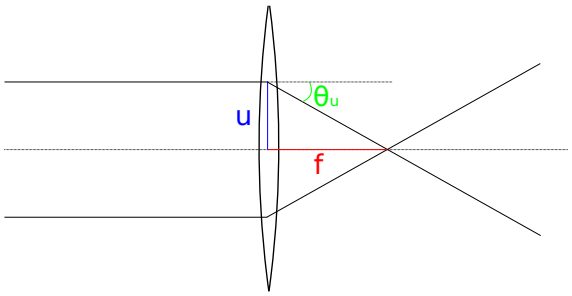

Figure 2.1: Thin lens approximation of a quadrupole.

then equation 2.2.3 becomes,

$$\begin{aligned} \ddot{x} &= \frac{q}{m} B_z \dot{y} \\ \ddot{y} &= -\frac{q}{m} B_z \dot{x} \\ \ddot{z} &= 0 \end{aligned} \tag{2.2.5}$$

These equations describe a circular motion of radius ρ. By introducing the inferred solution in the equations, introducing the momentum of the particle p, we find :

$$B\rho = \frac{p}{e} \tag{2.2.6}$$

Motion in a transverse quadrupole field Consider now a particle going through a quadrupole field.

$$\overrightarrow{B} = g \cdot d \cdot \hat{e}_z \quad , d = \sqrt{x^2 + y^2},\ g = \tfrac{\partial B_z}{\partial x} \tag{2.2.7}$$

then equation 2.2.3 becomes,

$$\begin{aligned} \ddot{x} &= \frac{q}{m} g \cdot d \cdot \dot{y} \\ \ddot{y} &= \frac{q}{m} g \cdot d \cdot \dot{x} \\ \ddot{z} &= 0 \end{aligned} \tag{2.2.8}$$

Let us consider a small quadrupole, such that $d \approx d_0 = cst$. Within this approximation and considering particles with small transverse momentum compared to longitudinal, the field seen by the particle is constant, as $x \sim cst$ and $y \sim cst$. We find back the dynamics of particle in a dipole field. As the motion is then circular, we have $\dot{x} = -\dot{y}$. Moreover, the movement in the z direction is trivial, we have that $dz = \dot{z} \cdot dt$. , we therefore introduce $p \approx m\dot{z} = cst$. We can then transform the last equations.

$$\left(\frac{p}{m}\right)^2 \frac{d^2u}{dz^2} \pm \frac{p}{m}\frac{q}{m} \cdot g \cdot d_0 \frac{du}{dz} = 0 \tag{2.2.9}$$

Where we used $u = x, y$ and took the upper sign for the horizontal plane and the lower one for the vertical. As the transverse momentum is small, we can define the transverse angles $\theta_u \approx \frac{du}{dz}$ (fig. 2.1). We also define the quadrupole strength.

$$k = \frac{1}{p}\frac{\partial B_z}{\partial x} = -\frac{1}{p}\frac{\partial B_z}{\partial y} \tag{2.2.10}$$

then we find the equations for the transverse angles :

$$\frac{d\theta_u}{dz} \pm q \cdot k \cdot d_0 \theta_u = 0 \tag{2.2.11}$$

Solving these equations, we find the change in transverse angles undergone by a particle going through a small quadrupole.

$$\theta_u = \pm \int q \cdot k \cdot d_0 \cdot dz \tag{2.2.12}$$

Such a behaviour is analogous to a light beam going through a lens. Indeed according to figure 2.1, particles entering the field normally with respect to the lens plane are focused at at a focal length f.

$$tan(\theta_x) \approx \theta_x = \frac{x_0}{f} \tag{2.2.13}$$

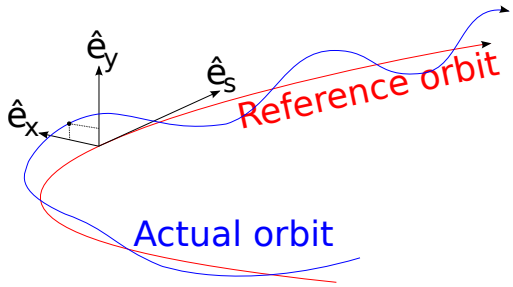

Figure 2.2: Schematic of the standard curvilinear coordinate system.

using the equation for the transverse angles, introducing the total length of the quadrupole L, we have :

$$\frac{1}{f} = q \cdot k \cdot L \tag{2.2.14}$$

In the y plane, we obtain the opposite result, showing that a quadrupole magnet has both a focusing and a defocusing plane. This approximation is known as the thin lens approximation and is widely used to treat big accelerators, in which the magnet size is negligible compared to the machine size. It is possible however to obtain the equation of motion for a long quadrupole by considering juxtaposition of small quadrupoles. Indeed, by differentiating equations 2.2.12 using the definition of θ and replacing $d_0 \to x(s)$, we find :

$$\frac{d^2u}{ds^2} \pm q \cdot k \cdot u = 0 \tag{2.2.15}$$

It can be shown that a dipole field also have a non null focusing strength. However this term is in the order of ρ^{-2} and can therefore be neglected in big accelerators like LHC.

Motion in a transverse sextupole field Consider a sextupole field :

$$\overrightarrow{B} = g' \cdot (x+y)^2 \hat{e}_z, g' = \frac{\partial^2 B_z}{\partial x^2} \tag{2.2.16}$$

Following the same reasoning, we find that the focusing provided by a sextupolar field is dependent on the position x.

$$\frac{1}{f} = q \cdot k_3 \cdot L \cdot x \tag{2.2.17}$$

where $k_3 = \frac{1}{p} g'$ is the sextupole strength and L the length of the magnet.

2.3 Accelerator magnet types

In particle accelerator physics, we use the concept of perfect dipole, quadrupole, sextupole and higher order magnets. They provide the design field along the reference orbit. In this approximation, the orbit is completely defined by the strength and position of the dipoles. The convention is that, unless stated otherwise, the magnetic field of the dipoles is vertical. In higher order magnets, the field on the reference orbit is null, therefore the orbit is straight. Quadrupoles and sextupoles are referred to as focusing and defocusing according to their action in the horizontal plane and act the opposite way in the vertical plane. Skew magnets of order n are placed with a $\pm\pi/(2n)$ angle with respect to the horizontal plane. Let us first describe the transverse dynamics of the particles considering an accelerator made of perfect magnets and then look at the effects arising from the the imperfections of the real magnets.

2.4 Curvilinear coordinate system

In order to describe the particle motion, it is useful to introduce the conventional curvilinear coordinate system described on figure 2.2. It is a Cartesian coordinate system centred on the reference orbit with the first axis $\hat{e}_s$ being tangent to the reference orbit, the second axis $\hat{e}_x$ perpendicular to $\hat{e}_s$ in the horizontal plane, pointing to the outside of the accelerator and the third $\hat{e}_y = \hat{e}_s \times \hat{e}_x$. This coordinate system simplifies the equations, therefore the understanding, as it intrinsically contains the geometry of the system.

2.5 Transverse dynamics

The trajectory of a single particle can be computed based on the equation described above. However, a beam is composed a set of particles with properties slightly different from the design ones. In particular, the positions and momentum of the particles in the beam are spread around the design values. In order to be able to store the maximum amount of particle in the machine, it is important to understand and control the motion of such a set of particle, even without considering the interaction between the particles.

2.5.1 Betatron motion

Let us describe the dynamics of particles with the design energy but slightly displaced from the reference orbit. In a particle accelerator made of dipoles only, such particles will quickly deviate from the reference orbit. Considering a beam of particles, each particle would be going away from the reference orbit, corresponding to a divergence, similar to the one of a light beam. The study of the quadrupole field showed that quadrupoles can be used as lenses. Noticing that the effect of alternate focusing and defocusing quadrupoles can be globally focusing, a proper set of quadrupoles along the trajectory may be used to focus and defocus the beam such that the beam never diverge.
Because of its similarity with an optical system, the definition of the position and strength of the quadrupoles and higher order magnet is referred to as the optic.

Equation of motion Let us consider a machine composed of dipoles and focusing and defocusing quadrupoles only. The orbit is defined by the disposition and strengths of the dipoles, its circumference is C. It is then possible to compute the transverse equation of motion around the reference orbit in the approximated machine based on the definition of the optics. Indeed, we can describe the optics by a periodic, piecewise constant function defining the quadrupole strength along the orbit :

$$K(s) = \begin{cases} k_m & \text{inside quadrupole } m \\ \dfrac{1}{\rho^2} & \text{inside a dipole} \\ 0 & \text{elsewhere} \end{cases} \qquad K(s+C) = K(s) \tag{2.5.1}$$

According to the equation of motion in a quadrupole field (2.2.15), we can write the equation for the displacement with respect to the reference orbit in both horizontal and vertical plane :

$$\frac{d^2u}{ds^2} \pm q \cdot K(s) \cdot u = 0 \tag{2.5.2}$$

which is well known as the Hill equation. It admits a solution of the type :

$$u(s) = a\sqrt{\beta_u(s)}\cos(\phi_u(s) - \phi_u(0)) \quad , \phi_u(s) = \int_0^s \frac{dS}{\beta_u(S)} \tag{2.5.3}$$

Which describe an oscillatory motion around the reference orbit with varying amplitude, known as the betatron motion. We have introduced the β_u function and the phase advance ϕ_u. Introducing the inferred solution back in the Hill equation, we find a differential equation for the β function.

$$\frac{1}{2}\beta_u\frac{d^2\beta_u}{ds^2} - \frac{1}{4}\frac{d\beta_u}{ds}^2 \pm q \cdot K \cdot \beta_u^2 = 1 \tag{2.5.4}$$

Therefore, the motion of the particle performing betatron motion around the orbit can be determined by solving this equation for the β function.

Transverse beam size The spread in position in the transverse plane is in general well described by a Gaussian distribution with standard deviations (σ_x, σ_y). As each particle is following the betatron motion, which is modulated with $\sqrt{\beta}$, the size of the beam along the trajectory vary accordingly.

$$\sigma_u \propto \sqrt{\beta_u} \tag{2.5.5}$$

Lattice optic Solving equation 2.5.4 for complex optics quickly gets painful, therefore the behaviour of the beam is more and more difficult to handle with increasing complexity. This motivates the introduction of a modular design. The machine is divided in cells with specific purpose that are independent of each other to the largest extend possible and with the simplest design.

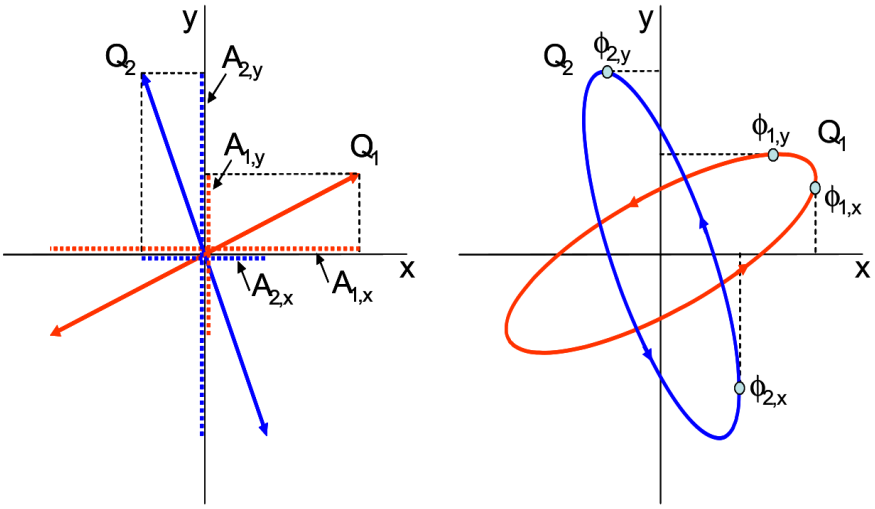

Figure 2.3: Schematics of coupled betatron motion. [7]

The FODO cell is the main component of an accelerator, it aims to maintain the beam focused around the orbit all along the accelerator. It is composed of a focusing and a defocusing quadrupole separated by either drift sections or dipoles. This way an accelerator can be composed of a sequence of identical FODO cells. The magnets composing the sequence are referred to as lattice magnets as opposed to insertions magnets. The insertions are a special set of cells, inserted in the FODO cell sequence. The set of cell inside the insertion is designed for a specific purpose such as accelerating particles, cleaning and measuring the beam or providing collisions. In the ideal case, the optics of the lattice are independent from the ones in the insertions. In the lattice as well as in the insertions, many corrector magnets are placed in between the main ones in order to account for the imperfections of each magnet.

Betatron tune Before going further in the design of the optics, let us define parameters that are useful for the characterisation of an accelerator. The betatron tunes $Q_{h,v}$ are defined for respectively the horizontal and vertical planes, they correspond to the number of betatron oscillation performed by a particle within one turn. They are computable from the β function.

$$Q_u = \frac{1}{2\pi} \oint_{\text{turn}} \frac{ds}{\beta_u} \tag{2.5.6}$$

The tune has a strong importance for the operation of an accelerator, as will be discussed in 2.9. Using the tunes and equation 2.5.3, we can write the position of a particle at a certain position s after n turns.

$$u(s,n) = A(s) \cdot \cos(2\pi Q_u n + \phi_u(s)) \tag{2.5.7}$$

Betatron coupling Until now we have considered the horizontal and vertical planes separately, as we have not considered the possibility of including skew elements nor solenoid fields. The theoretical treatment of the effect of such field can be found in [7]. As shown by figure 2.3, the result is a rotation of the oscillation planes and frequencies. Equation 2.5.7 becomes :

$$\begin{cases} x(n) &= A_{1,x}(s)\cos(2\pi \cdot Q_1 \cdot n + \phi_{1,x}(s)) + A_{2,x}(s)\cos(2\pi \cdot Q_2 \cdot n + \phi_{2,x}(s)) \\ y(n) &= A_{1,y}(s)\cos(2\pi \cdot Q_1 \cdot n + \phi_{1,y}(s)) + A_{2,y}(s)\cos(2\pi \cdot Q_2 \cdot n + \phi_{2,y}(s)) \end{cases} \tag{2.5.8}$$

where we can define the coupling amplitude $|C^-|$ and coupling phase χ such that :

$$\begin{cases} \dfrac{A_{1,y}(s)}{A_{1,x}(s)} &= \sqrt{\dfrac{\beta_y(s)}{\beta_x(s)}} \dfrac{|C^-|}{\sqrt{\Delta^2 + |C^-|^2} + \Delta} \\ \dfrac{A_{2,x}(s)}{A_{2,y}(s)} &= \sqrt{\dfrac{\beta_x(s)}{\beta_y(s)}} \dfrac{|C^-|}{\sqrt{\Delta^2 + |C^-|^2} + \Delta} \\ \chi &= \phi_{1,y} - \phi_{1,x} \\ \chi - \pi &= \phi_{2,y} - \phi_{2,x} \end{cases} \tag{2.5.9}$$

where Δ is the difference of the fractional part of the tune split $Q_{\text{split}} = |Q_h - Q_v|$. Q_1 and Q_2 are the eigenvalues, they coincide with the horizontal and vertical tunes in case of null coupling amplitude or null tune split.

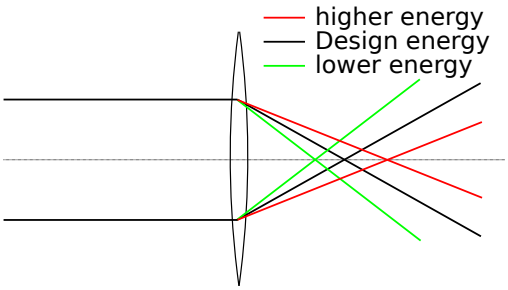

Figure 2.4: Schematic the chromaticity of a quadrupole.

2.6 Off momentum particle

Dispertion Looking at equation 2.2.6, we see that, for a fixed field, the bending radius depends on the momentum of the particles. As the particles consituing the beam have a spread in energy, their trajectories are different according to the energy of each particle. The trajectory of each particle with a momentum p differing from the design momentum p_0 can be described as a first order deviation from the reference orbit. Introducing the dispersion $D(s)$, we have :

$$\Delta x = D(s) \cdot \delta \quad , \delta = \frac{p - p_0}{p_0} \tag{2.6.1}$$

The dispersion in the vertical plane is null, as the trajectory is bend only in the horizontal plane. It is possible to minimise the dispersion generated in the circular section using specific sets of dipoles and quadrupoles, such a set is called a dispersion suppressor.
Dispersion is in general detrimental for the operation of an accelerator, mainly because the orbit deviation from the reference orbit of off-momentum particle may become too large to fit the aperture of the vacuum pipe.

Chromaticity Equation 2.2.10 shows that the focusing undergone by off-momentum particles is not identical to the design one. Keeping in mind the optical analogy, fig. 2.4, we define the chromaticity :

$$\xi = \frac{\partial Q}{\partial \delta} \tag{2.6.2}$$

The chromaticity has strong importance in the longitudinal dynamics, certain values of chromaticity can lead to resonant longitudinal motion known as head-tail instabilities. In particular, in high energy sychrotrons such as the LHC, negative chromaticity causes such instabilities that may lead to particle losses, and must therefore be avoided. Moreover, a large chromaticity implies that off-momentum particles have large tune deviation and may be lost because of tune resonances, which will be discussed in 2.9 .
The chromaticity of an accelerator made of dipoles and quadrupoles is negative, as a particle with higher momentum is less focused. This natural chromaticity has to be corrected in order to be positive, as small as possible. Sextupole magnets can be used to correct for the chromaticity as they provide a focusing that is dependent on the position. Therefore, by placing them in high dispersion region, such as the end of a dipole, it is possible to provide a focusing dependent on energy. Indeed, introducing 2.6.1 in 2.2.17, we have :

$$\frac{1}{f} \propto D(s)\delta \tag{2.6.3}$$

2.7 Luminosity

Together with the energy, the luminosity is the most important parameter of a collider. It is defined to characterize the rate of collision r that can be expected for a specific process of cross section σ.

$$r = \mathcal{L} \cdot \sigma \tag{2.7.1}$$

The luminosity depends on many properties of the beam at the IPs such as the beam shape and size, the crossing angle and the energy spread. A proper model of the luminosity is not trivial, in case of the LHC, studies are still ongoing to find the best one. However, we can get a good approximation by considering two bunched beams of cross section A with N particle per bunch colliding head on. With an average bunch collision frequency f, we find the luminosity :

$$\mathcal{L} = \frac{f \cdot N^2}{A} \tag{2.7.2}$$

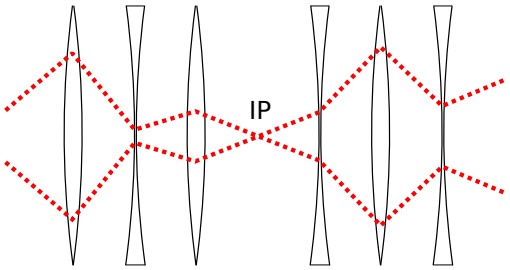

Figure 2.5: Schematic of the triplet assembly

This approximation provides the principal leads to maximize the luminosity of a collider. Optimizing for high luminosity by playing with those parameters is then a complex task, several limitations have to be taken into account. In the case of LHC, the final limitation is not yet fully understood, much effort is being undertaken to understand it and push it as far as possible.
To describe the collider performance, it is useful to introduce the integrated luminosity $\mathcal{L}_{\text{int}}$, such that the amount of events with cross section σ that can be expected is $\sigma \cdot \mathcal{L}_{\text{int}}$.

$$\mathcal{L}_{\text{int}} \equiv \int \mathcal{L}(t)dt \tag{2.7.3}$$

Indeed, the peak luminosity $\mathcal{L}_{\text{peak}}$ is attained when the beams are put in collision, then the luminosity decreases with time because of different processes that causes the degradation of the beam. The most obvious process is the burning of the particles that collided but other effects are also significant due to the so called beam-beam interaction. Once the beam is too degraded, it is extracted from the machine and replaced by a new one.
The maximisation of the integrated luminosity rely on the optimisation of many parameters, in particular the turnaround time, from the dump of the beams to the production of collision using the new ones, needs to be minimised. The maximisation of the operational efficiency is also relevant, in order to minimise the number of critical failure that would cause a premature dump of the beams.

Betatron squeeze Equation 2.7.2 shows that luminosity can be increased by reducing the beam cross section at the IPs. Assuming that the size of the beam is equal in both planes, we have :

$$\mathcal{L} \propto \frac{1}{\beta^*} \tag{2.7.4}$$

where β^* is the β function at the IP.
Maintaining small β function all along the accelerator is difficult to achieve as it requires a lot of focusing strength. However, the β function can be chosen such that the beam size fits the aperture of the accelerator along the ring and minimized at the IPs using a specific set of quadrupoles. The operation of lowering the beam size at the IPs by acting on the β function is known as betatron squeeze.

Triplet assembly In order to perform the squeezing of the beam, a specific set of quadrupole is disposed symmetrically around the IP. Fig.2.5 shows the three magnets closest to the IP using the optical analogy. It clearly shows that, in order to obtain low β regions, the β function has to be made very large in these particular magnets known as the triplets. This effect quickly becomes a limitation as the beam size in the high β regions must still fit the aperture.

2.8 Collimation

Perfect storage of the beam can never be achieved in a real machine. In high energy accelerator, and most importantly the ones using superconducting technology, the particles lost have to be handle with great care. Indeed, high energy particles that are lost will eventually deposit their energy in the surrounding material, possibly causing important damages. In particular, the heat load can be detrimental to superconducting magnets operating at very low temperature. To prevent the losses to appear randomly around the machine, a collimation system can be installed. It aims to catch all particles that are too critical and would likely be lost around the machine otherwise. Particle performing too large amplitude betatron motion have to be cleaned as they could hit the vacuum chamber's wall. This can be done by inserting an absorbing material closer to the beam than any other element of the machine to catch them. To achieve higher cleaning efficiency

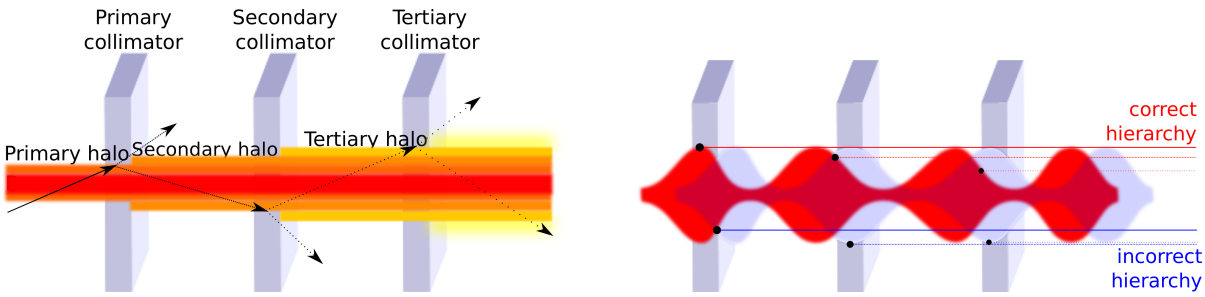

(a) Principle (b) Sensitivity to β_{beat}

Figure 2.6: Three stage collimation system. In (b), the blue beam is subject to large β_{beat}, causing the hierarchy of the collimator to change, therefore reducing the efficiency of the system. Similarly, orbit distortions are detrimental to the efficiency of the cleaning.

it is possible to insert multiple stage of absorbing material such that particle hitting one stage without being absorbed would nevertheless be deviated and possibly be absorbed by the next stage. As shown by figure 2.6, such a collimation system is highly sensitive to the beam position and size at the position of the collimators.

2.9 Field errors

Numerous field imperfections have to be taken into account in a real machine, which breaks down into two categories.

Misalignment Misaligned perfect magnets have different effects on the beam, depending on the type of misalignment and the type of magnet. A magnet misaligned in the transverse plane is well described by the superposition of lower order magnets on top the the perfect one, as can be shown by introducing the new transverse coordinate $x \to x + x_0$ in the equation of the different transverse multipole field. In a more subtle manner, yaw and pitch angles error have a similar effect. It is then important to note that these imperfections do not affect the dipoles from the beam dynamics point of view. However a roll angle error has its importance for any magnet, as it corresponds to a rotation of the transverse plane, therefore generating coupling.

As an example, the field felt by a particle through a quadrupole displaced by δ_x along the x axis is equivalent to the superposition of a perfect quadrupole and a dipole with a bending radius ρ.

$$\rho = \frac{1}{p}\frac{\partial B_z}{\partial x}\delta_x = k \cdot \delta_x \tag{2.9.1}$$

Multipole error The field produced by a magnet depends on the coils shape, current distribution and also on the surrounding materials. Imperfections in these parameters can lead to several inhomogeneities in the field. The real field can then be described by the superposition of multipole magnets with low strength compared to the main component.

Resonances The particles are circulating on a circular trajectory, therefore going through a similar environment from turn to turn. Resonances may arise from this periodicity, as an example, let us consider a misaligned quadrupole in an otherwise perfect circular machine. The dipole field thus generated will introduce a kick of angle θ at the position of the quadrupole s_0, it can be shown that the orbit will then deviate from the reference according to the following equation using a perturbative approach [6].

$$u(s) = \frac{\theta\sqrt{\beta_u(s)\cdot\beta_u(s_0)}}{2\sin(\pi Q_u)}\cos\left(\phi_u(s) - \pi Q_u\right) \tag{2.9.2}$$

It appears that for an integer tune, the orbit goes to infinity, which clearly goes beyond the perturbative treatment. However, this shows that the circular motion is no more stable in such an accelerator, no matter how small is the kick. Considering a very general accelerator, tune resonances can appear if the tunes are such that :

$$m \cdot Q_h + n \cdot Q_v = p \quad , m, n, p \in \mathbb{Z} \tag{2.9.3}$$

The importance of these resonances is decreasing for increasing order $o = |n| + |m|$.
Equation 2.9.2 has another important implication if the tune is off resonances. Indeed, the amplitude of the orbit deviation created by the kick depends on the β function both along the machine and at the kick position. Thus the beam become more sensitive to dipole field error as the β function is high.

β_{beat} Field errors also have an impact on the optic. Indeed, parasitic quadrupole field have to be taken into account for the calculation of the β function. The deviation of the real β function to the nominal one is expressed using the β beating coefficient β_{beat}.

$$\beta_{\text{beat}} \equiv \max_{s\in[0,C[} \left| \frac{\beta_{\text{real}}(s) - \beta_{\text{nominal}}(s)}{\beta_{\text{nominal}}(s)} \right| \tag{2.9.4}$$

β beating is detrimental for numerous reasons, among them, the collimation efficiency may be the most critical. Indeed, as seen in section 2.8, the collimation system heavily rely on the knowledge of the beam size at the position of the collimators. Moreover, it can lower the luminosity by inducing a higher β function at the IP, therefore a bigger beam size.

Chapter 3

The Large Hadron Collider

In this section, I will present the main properties of the LHC, adopting the point of view of the operator. That is to say that details about the implementation will be given if they are relevant for the operation of the machine.

3.1 Layout

As shown on figure 3.2a, the LHC ring can be divided in octant, each composed of an arc and an insertion. An arc is composed of 23 FODO cells, each built as described in figure 3.2b. The lattice quadrupoles are disposed in the so-called short straight section, along with an orbit corrector, a normal and a skew quadrupole corrector and the lattice octupoles. In between each short straight section, three main dipoles are placed separated by sextupole, octupole and decapole spool-piece corrector magnet. Each insertion has its own purpose, as shown by figure 3.2c, they are all designed in a similar manner. There are four sets of components. From the arc to the centre of the insertion, the beams go through some trim quadrupoles, a dispersion suppressor assembly and a set of matching quadrupoles before entering the specific components of the insertion. This design allows to minimise the dispersion generated in the arcs and to decouple optic of the arcs from the specific components in between the matching sections (MSs). The implementation of the different elements is specific to each insertion in order to fit the requirements of each system [8]. In the case of squeeze, we will be mostly interested in the layout of the insertions where experiments are based, that is to say where collision happens.

Experiments regions ATLAS and CMS are both high luminosity experiment, they are located at opposite sides of the ring, the only difference in the optic of the two insertions is the crossing angle plane. Whereas the crossing angle is vertical in ATLAS, it is horizontal in CMS. Figure 3.2c shows the common layout of the magnet in the colliding insertions. In between the MSs, the beams are put in collisional orbit by the separation/recombination dipole magnets, the one closer to the IP being a normal conducting one. The final focusing is provided by the triplets, which are single aperture superconducting quadrupoles, this implies that both beams goes through the same field.
Insertions 2 and 8 are used for the two lower luminosity experiments, ALICE and LHCb and for the injection of beam 1 and 2 respectively. The optics of these insertions is very similar to the other colliding insertions

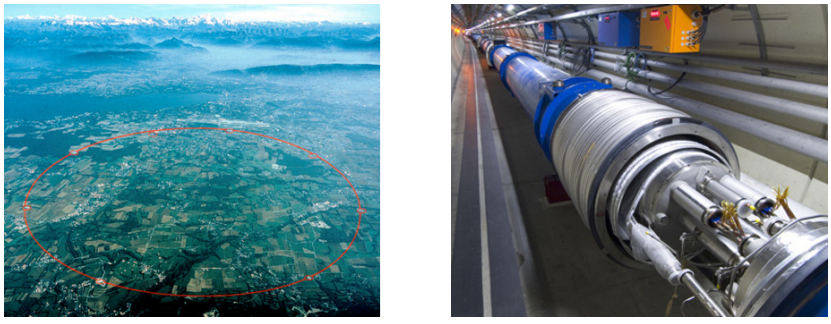

(a) Form the sky (b) Inside the tunnel

Figure 3.1: The LHC ring.

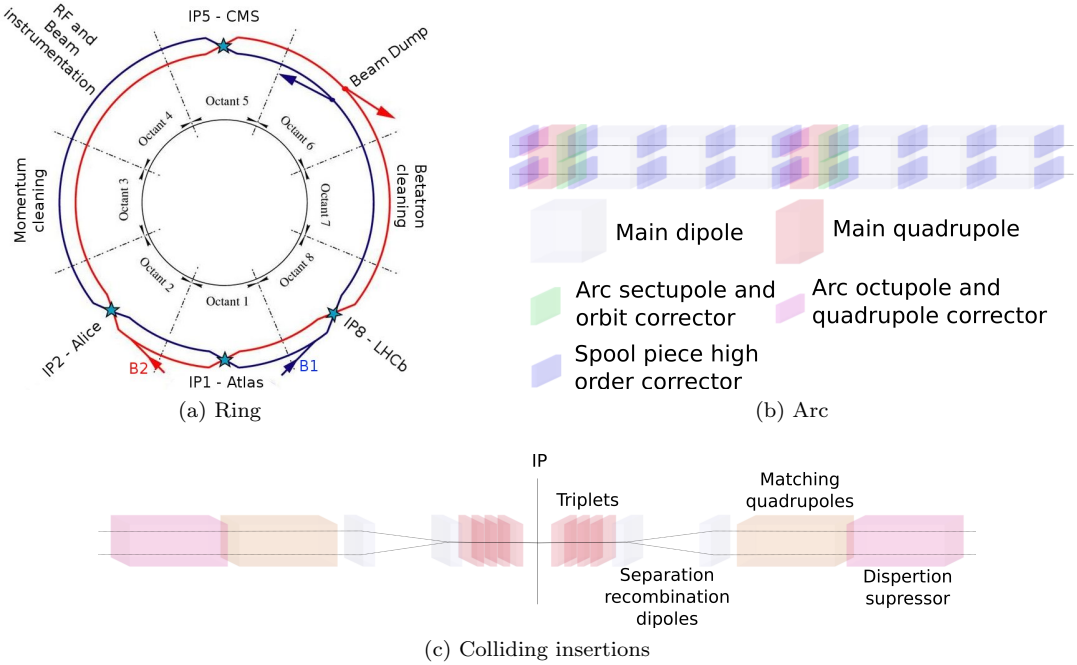

(a) Ring (b) Arc

(c) Colliding insertions

Figure 3.2: Simplified schematics of the LHC Layout.

except from the room left for the injection. Moreover, profit has been taken from the lower radiation level in these experiments to replace the normal conducting separation/recombination magnets by superconducting ones.

3.1.1 Correction schemes

Orbit In order to properly correct the orbit, the LHC uses 530 kickers per plane, 376 of them are located in the arcs. The orbit can be either steered manually or controlled continuously by the orbit feedback system (OFB). Based on the data provided by the beam position monitors (BPMs), the OFB uses fitting algorithms to find the best correction applicable with the available correction magnets.

tune To act on the β function, the LHC possesses 440 quadrupole correctors, 320 of them are located in the arcs. In addition, 72 skew quadrupoles are used to correct for coupling. These magnets could be used to locally correct the optics, but they are mainly used to globally correct tune and coupling. Correction up to $\Delta Q \sim 0.1$ units can be achieved by this correcting scheme. A tune feedback system (QFB) is used to stabilise the tune during operation. The QFB has shown to be able to maintain the tune within less than 10^{-3} units deviations from the nominal tune, within a response time in the order of the second [9]. Even though coupling and chromaticity feedback systems are apart of the design of the machine, they have not been commissioned yet. This has a detrimental effect on the QFB, as it can not operate with high coupling, therefore coupling has to be properly corrected manually during operation.

Chromaticity 2472 spool piece sextupole corrector and 688 lattice sextupoles are used to compensate the sextupole field error arising from lower order magnet and the natural chromaticity (~ 100 units) respectively.

3.2 Magnets

To control the beams, the LHC uses several types of magnets, from the main bending dipoles to dodecapole spool-piece correctors. They share key properties that are described below [8].

3.2.1 Basic specificities

The arc magnets and most of the insertion ones are superconducting, based on Nb-Ti technology. The exceptions are magnet located close to the IPs or in the cleaning insertions, the heat load generated by the heavy radiations would cause the magnet to quench too often. Fast magnets, like extraction kickers, are

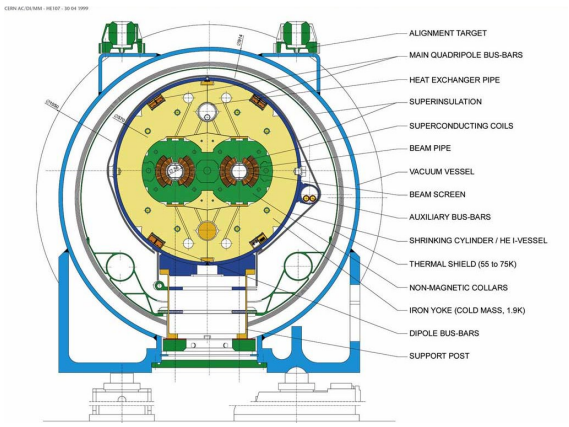

Figure 3.3: Diagram of LHC main dipole and cryostat.

also non-superconducting magnets. I will focus on the description of the superconducting magnets as the operation of the machine is mostly limited by their specificities.

The LHC magnets are the results of several years of research, they are able to create high magnetic fields with remarkable accuracy and stability. The superconducting nature of the magnets has however some features that limits the operation and have to be taken into account. [10]

Resistive transition The superconducting nature of the magnets is highly dependent on the temperature and the magnetic field produced. An increase of the temperature can cause the material to become resistive. Typical current in the LHC magnets are in the order of kA, therefore storing a huge amount of energy. This energy cannot be allowed to be dissipated in the magnet coils, as it would cause them to melt. Therefore, resistive transitions, also known as quench, are extremely detrimental to the operation of the machine. The LHC is equipped with a quench protection system (QPS), which aims to detect resistive transitions in the superconducting magnets and immediately evacuate the energy that it contains. The missing magnet compromises the operation of the machine, the beam is therefore dumped when a quench is detected.

Hysteresis Both the hysteresis of the magnet and of the iron yoke plays an important role in the total field felt by the beam. The nature of hysteresis in superconducting magnet of Type II, such as Nb-Ti magnets, is quite different from normal conducting magnets. In Type II superconducting materials, normal conducting filaments form inside the material. In this filament high fields can exists, whereas the field penetrate the superconductor only on short distance. In order to attenuate the field inside the material, current loops appear around the filaments to balance out the field inside the superconductor. As the resistance of the material is null, these currents are persistent and therefore cause an hysteresis. This effect is not a priori detrimental to the operation, but proper models must be introduced to include it in the computation of the current in the magnets [11].

Decay and snap back effect Decay and snap back effects, however, have a much more detrimental effect on operation. Even though persistent currents are highly suspected to be the cause of these effects, they are not yet fully understood. It is observed that, while operating at constant current, the superconducting magnets will show a slow decay of its field. This field will then be quickly recovered when the current is changed. Decay typically happens during the injection, during which the field of most magnets is fixed, snap back will then appear at the beginning of the energy ramp. There were many concerns during the design of the machine about these effects, most importantly, their random nature could render the operation of the machine impossible without proper correction systems.
These effects are intrinsic to the superconducting magnet technology, therefore they can not be fully avoided. However, it was found that they have a strong dependency on the powering history of the magnets, which lead to the introduction of precycles. The precycles are functions that are systematically run by each magnet before each fill of the machine, allowing to have a similar powering history for each run. The reproducibility is therefore improved, allowing an easier understanding of the machine and a minimization of the needs for feedback systems.

Derivative limitations The current in the superconducting magnet cannot be varied arbitrarily, there are constrains on both first and second derivatives of current as a function of time. The speed of the operation is

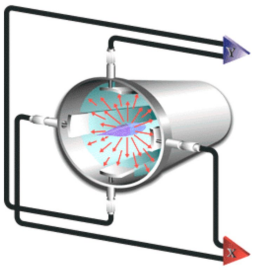

Figure 3.4: Beam position measured by a strip line BPM.

mostly limited by the first derivative constrain, as this defines the ramping rates of the magnets. The most important limitation comes from the main dipoles, whose ramp rates can not exceed 10 A/s. Therefore, the ramp from injection energy to 3.5 TeV takes 17 minutes. The second derivative limitation has a more subtle consequence on operation. Indeed, it implies that the current functions that the magnets should follow must have specific shapes that fits this limitation, rendering certain operations, like the immediate stopping the ramping of a magnet impossible.
The immediate effect of the violation of these limitations is the appearance of a non null voltage in the superconducting cables. This voltage is interpreted as a quench by the QPS that will then trigger a dump of the beam.

Modelling The measure of the current in the magnet coils is available all along operation, however the computation of the corresponding magnetic field that is felt by the beam requires a good knowledge of the behaviour of the superconducting material, of the geometry and other specificities of each real magnet. In order to model the field from the current in the magnets, the Field Description for the LHC (FiDeL) [10] is used. The implementation of the model is already at an advanced state. Even though its is not complete, the current implementation allows an operation of the machine in good conditions.

Powering The power of the grid is transformed by power converters (PCs) to produce the high current needed by the superconducting magnets. The PCs are large and expensive piece of equipment, therefore their number has to be limited for both questions of price and room in the tunnel. Several magnets assuming identical function, as the dipoles in the arc for example, are powered in series.
In order to both fit the requirements of the superconducting magnets and the operational needs, the PCs are operated the following way. The current as a function of time can be loaded in each PC, such that the current is varied from the existing current to another value in a finite time span, respecting the magnets specificities. When its is triggered, each PC executes its function, rejecting new instructions for the duration of the function except from the QPS. Except a specific subset of PCs, such as the ones powering dipole and quadrupole corrector, that remain open to new commands by the feedback systems.

3.3 Beam measurements

The LHC's diagnostics systems are being commissioned progressively during operation, I present here the systems operational at the end of the 2010 run.

Orbit The orbit is measured all along each beams by 516 BPMs. Their are several types of BPMs with various specificities that can provide different diagnostics. They all provide bunch by bunch information on the beam position in both horizontal and vertical planes. They work on the principle shown by figure 3.4, four so-called pick-up electrodes are placed symmetrically around the beam, the analysis of the signal induced by the passage of the beam provides the position of the beam in the transverse plane. The main differences among the BPMs are in the quality of the electronics for the signal treatment. The standard BPMs can provide turn by turn measurement of the beam position with a resolution of 50μm or 5μm when averaging over 224 turns. [8]

Tune Introducing the phase advance after n turn $\phi_u(s) = 2\pi \cdot Q_u \cdot n$ in equation 2.9.2 :

$$u(s,n) \propto \cos(2\pi \cdot Q_u \cdot n + cst) \tag{3.3.1}$$

we observe that, in the presence of a dipole imperfection, the transverse position of the beam measured at a fixed position along the ring oscillates at a frequency that depends on tune. Therefore the signal induced

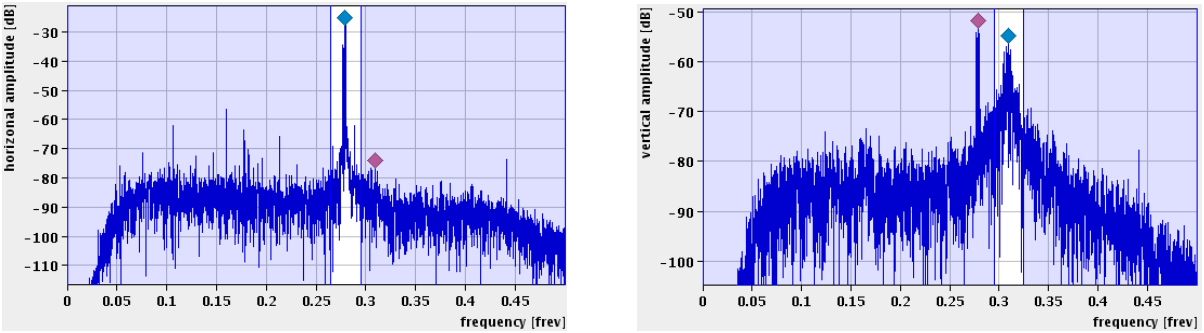

(a) Horizontal (b) Vertical

Figure 3.5: Example of tune spectrum measurement in both planes. The dots shows the measured eigenvalues, the blue one correspond to the the eigenvalue closest to the tune in the measurement plane.

in a BPM will contain these oscillation components. It is therefore possible to obtain the so-called tune spectrum by using Fourier decomposition of the BPM signal. An example of tune spectrum measurement at the LHC is shown in figure 3.5. It is non null only in the presence of imperfections, as there would be no orbit oscillation otherwise. In practice there are many sources of imperfections that will excite the beam in a wide range of frequencies, such as noise in the power supplies or ground vibrations. The tune spectrum is then populated with many frequencies. This method rely on the fact that the main component comes from the betatron motion frequency and its harmonics. It is indeed observed on figure 3.5. As described in [9], the detection of the tune signal is not a trivial task and is ensured by the base band tune (BBQ) system. Whereas an extra excitation of the beam was required with older systems, the BBQ allow one to obtain a tune signal strong enough without extra excitation. Its first limitation, however, remain the weakness of the tune signal. Indeed, as it relies on peak detection in the tune spectrum, the probability of detecting the wrong peak strongly depend on the signal to noise ratio. In most cases, a resolution in the order of 10^{-5} can be expected [9].

Coupling In an uncoupled machine, the measurement of the tune can be performed in both planes using separately the horizontal and vertical tune signal. However, this is not applicable in the presence of coupling. The betatron motion of a coupled accelerator happen on tilted planes with different frequencies defined by the eigenvalues Q_1 and Q_2. Therefore the main components seen on the horizontal and vertical tune spectra will be the eigenvalues. However, they will both appear in both planes, with different amplitudes. The amplitude of the signals can be used to measure the coupling via equation 2.5.8. This measure can then be used to compute the horizontal and vertical tunes from the eigenvalues.
It is important to note that, as the coupling is kept as low as possible, the amplitude of the signal of Q_1 in the vertical plane and Q_2 in the horizontal are very weak. Therefore, for the same reason as the ones described in the case of the tune measurement, the measurement of the coupling is strongly dependent on the signal to noise ratio and is often imprecise. The tune spectrum in 3.5 shows the signature of a high coupling, as the horizontal tune peak is clearly visible in the vertical spectrum.

Chromaticity Observing the definition of the chromaticity, the most straight forward measurement method is to slightly vary the energy and measure the resulting change in tune. Continuous measurement of the chromaticity is then detrimental for the operation of the machine, as it requires continuous variation of the energy. Therefore this method is mostly used for on-demand measurement, but is also used for continuous measurement for specific analysis on rare occasions. The resolution of the measurement strongly depends on the resolution of the tune measurement, and the amplitude of the energy modulation. In the current state, a resolution better than 1 unit can be expected [12].

Intensity The intensity of the beam is defined as the number of charges that it contains. The number of charge can be measured via the measure of the electric current flowing through the vaccum chamber. This current is measured by beam current transformers (BCTs), they use the measurement of the magnetic flux induced by the passage of the beam through a toroidal core. The BCT installed at the LHC allows bunch by bunch measurement of the intensity with an accuracy of 5% [13].

Losses 4000 beam loss monitors (BLMs) are installed just outside the beam pipe in warm regions and outside the cryostat in cold regions. A BLM is an ionization chamber that measures the energy deposition

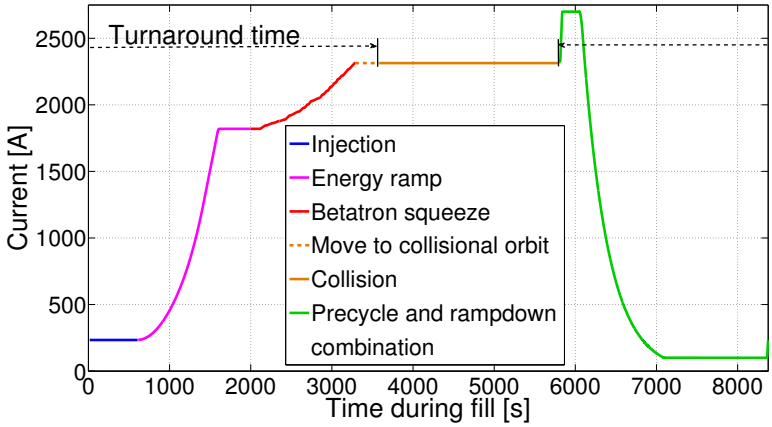

Figure 3.6: Schematics of the current in a selected matching quadrupole during a standard operation cycle.

of secondary particles resulting from the collision of particles from the beam with the walls of the vacuum chamber. This method do not allow to measure the intensity that is lost, however a proper calibration allow to compute the heat load expected in the cryostat, taking advantage of the linearity of the BLM signal with the intensity of the beam. As the BLMs are spread along the ring, they allow to localise the losses. Moreover, each BLM provide average losses over time scales from 40μs to 80s, therefore allowing to localise slow and fast losses in time. This has an important role to play in the QPS, that is thus able to trigger a dump of the beam when significant losses are observed, before the heat load causes a quench of the magnet.

3.4 Operational aspects

The operation of the LHC and its injector chain is done from the CERN Control Centre (CCC) in Prévessin (FR).
A lot of unknown remains after the design and construction of the machine, they are being unravelled by the observation of the behaviour of the machine with a circulating beam. It is clear that a good operation is the result of many systems interacting, each of them has to be well understood in order to insure its proper usage.

3.4.1 Standard operation cycle

In standard operation, the machine is run in consecutive cycles, referred to as fills, shown on figure 3.6. The machine is first prepared to be filled, this operation includes notably the precycling of the magnets. The LHC is then filled with particles at the injection energy, the orbits being kept separated in all IPs. The energy of the beams is then ramped to the top energy, before performing the squeezing. Depending on the demands of the different experiments, the squeeze can be performed in different manners. In some cases, the squeezing can even be skipped. The orbit are then brought together to produce collisions until the beams are extracted. The dumping of the beams can be triggered during the whole cycle by control systems such as the QPS or manually, when the quality of the beams become too low to produce high luminosity. Before restarting the cycle, magnets are ramped down. In general, the precycling is combined with the ramp down in order to save time. Each of these operations have their specificities and are under constant improvement.

Reproducibility In such a defined cycling, the machine could be expected to show similar behaviour from one fill to another. This is possible assuming a reproducible behaviour of each component of the machine, including its injector chain. Especially during commissioning, a strictly identical operation cycle can not be respected, as systems are being commissioned step by step. Even during standard operation, many source of time dependent disturbance are to be expected, such as noise in the different powering systems or ground motion. Moreover, the field produced by the magnet depends on their powering history. Mostly because of decay and snap back effects, the reproducibility of the machine was not expected to be as good as it is observed. Feedback systems are introduced to control the most important beam parameter such as orbit, tune, coupling and chromaticity.

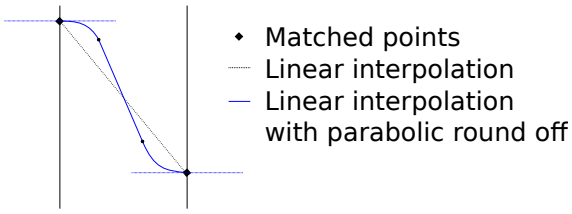

Figure 3.7: Generation of the settings of an hypothetical parameter in between two matched points.

3.4.2 Settings management

The LHC software architecture (LSA) [14] is the software responsible of handling the settings of most of the LHC's equipments, the operation of the machine is therefore completely dependent on its implementation, some relevant features are described below.
During some of the operations described above, the current of the magnets have to be changed according to a specific purpose, in a synchronous manner. The concept of beam process (BP) is introduced to encapsulate the settings of all the element in the machine while executing the desired operation. In particular, the BP contains all the functions that describe the current of each PC in the machine for the time span needed to perform the operation. Therefore, it is possible to load all the function in all the PC and then trigger them simultaneously. The machine is then blocked for duration defined by the BP. Each BP therefore contains an enormous quantity of information computed in advance and allow to operate in a reasonably simple manner a machine composed of thousands of magnets.

Correction and knobs The optics are defined based on the current knowledge of the machine. However, this is not sufficient for a proper operation of the machine, as several imperfections are still unknown. Corrector magnets can be tuned to compensate the imperfections, based on the measurements that are available. Operating each corrector at a time would be a Herculean task, the correction schemes are therefore hidden behind the concept of knobs. A knob translate a change in a high abstraction parameter into the change of strength of each corrector magnet that is used to perform the desired changes using the specific correcting scheme. As an example, in order to change the tune of an accelerator, the whole optic has to be changed. However, using the tune knob allow the operator to change the tune without having to care about each quadrupole corrector. The value of the different knobs as a function of time is also stored in the BP.

3.4.3 Betatron squeeze

As discussed in section 2.9, the machine gets more and more sensitive with higher β functions. Therefore the squeeze is a delicate operation, and simple linear interpolation of the magnet strengths from the injection optic to the squeezed one is not sufficient. Indeed, the deviation from the nominal machine arising from the linear interpolation of each strength can have significant impact on the operation of the machine. In order to achieve the total squeezing more smoothly, it is done part by part. Several optics are defined as intermediate steps, referred to as matched points (MPs), allowing a smooth transition between the two extreme optics. This procedure however has a cost. Indeed, as discussed below, the generation of valid functions for the magnets necessitate the introduction of slow round off at each MP, therefore increasing the length of the squeeze and consequently the turnaround time, which is detrimental to the integrated luminosity.
The introduction of MPs has a second advantage. Indeed, because of the specificities of the superconducting magnets, the MPs are the only point at which it is possible to interrupt the BP during its execution. This feature is extremely important to allow punctual measurements and corrections during the squeeze, especially during the commissioning phase. Indeed, the continuous measurement and correction of certain parameters are still not available, during the first squeeze, none of them were. Therefore, the only possibility to introduce a correction during the squeeze is to stop to perform on-demand measurements and apply the appropriate corrections.

Generation The generation of squeeze BPs is based on the definition of optics at different times. These optics have been developed in order to obtain a machine that matches perfectly the nominal characteristics. In between theses matched optics, the strength of each magnet is interpolated linearly, taking into account the maximum ramp rate of each magnet. The function obtained is not valid for operating a superconducting magnet, as it contains discontinuities at each MP, as the derivative can potentially be different before and after. The FiDeL model is then used to compute a valid function, taking as a condition that it should be possible to stop at each MP. Parabolic round off are introduced in order to have a zero derivative of each

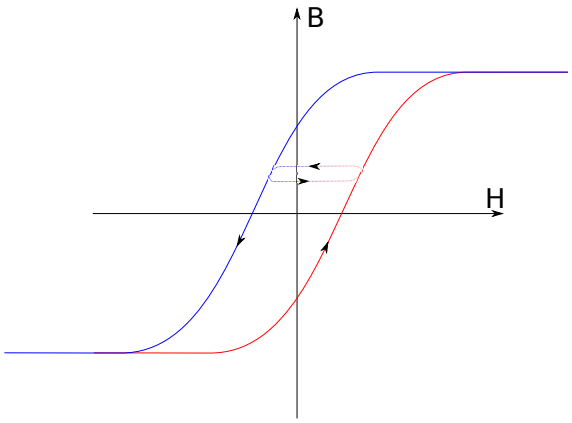

Figure 3.8: Current model of the hysteresis of the main magnets.

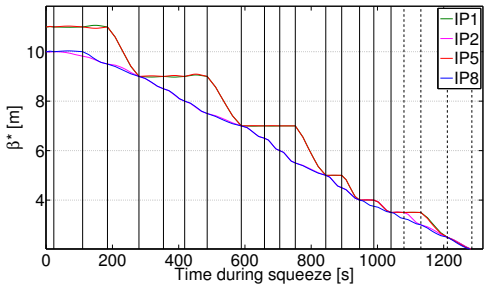

(a) β^* evolution

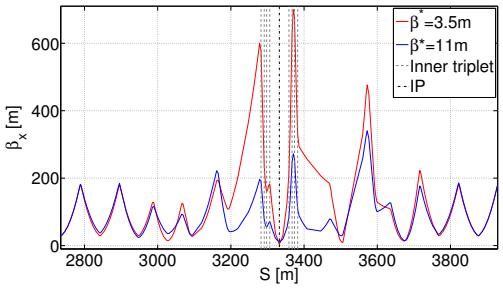

(b) Horizontal β function around IP1 before and after.

Figure 3.9: Simulation of the β^*s during the execution of the squeeze BP used in 2010 for both protons and ions. Squeezing beyond 3.5m was abandoned early during the run.

parameter at the matched optics. The optics in between the MPs are not matched, therefore the machine is expected to behave slightly differently to the nominal one. An example of the settings generated for a hypothetical parameter between two MPs is shown on figure 3.7.
While generating the settings of the PCs, other aspects of FiDeL has to be taken into account, as there is no one to one correspondence between the current in the coils and magnetic field produced. Along with other effects described by the transfer function of each magnet, the effect of hysteresis are included at this level. To account for this effect in particular, the current corresponding to the strength of each magnet is computed using calibration curves that are based on measurements performed before the assembly of the magnets. The current corresponding to a certain strength is then different while ramping up or down, the transition being done smoothly in the order of the second when changing derivative. This model (fig. 3.8) is approximative, the real behaviour of the magnetisation is more complicated. Indeed, both the magnetisation of the iron yoke and the superconducting strands have to be taken into account. Still this model allow to have a simple treatment of hysteresis in the generation of the settings.
The hysteresis in the corrector magnet is ignored. Indeed, most of the correctors are subject to manipulations on line by the feedback systems. The change of sign of the derivative can not be predicted and the implementation become much more difficult. Although the orbit and tune deviations expected from this mistreatment are beyond the tolerances [15], the feedback systems can correct for them.

2010 For the first physics run of the LHC, is has first been decided that all IPs would be squeezed simultaneously down to $\beta^* = 2$m. However, based on the first weeks of experiences, the squeeze was perform in all IPs to $\beta^* = 3.5$m. The number of MPs has been chosen to maximum, that is to say using all the intermediate matched optics that were available. This decision is motivated by the need to perform the commissioning of the squeeze in a short delay. Indeed, the large number of MPs insure minimal deviation of the beam parameters due to the unmatched optics, thus limiting the risk of exceeding the tolerances, which would require a significant amount of time for a proper correction. The optimisation of performances is not an issue in this first approach. Figures 3.9a, show the evolution of β^* in the different IPs, the position of the MPs is listed in table 3.1.
During the first 23s, no modification of the β^*s is performed. This time is used to change the tunes from their

t [s]	β^* [m]			t [s]	β^* [m]		
	IP1&5	IP2	IP8		IP1&5	IP2	IP8
0	11	10	10	752	7	5.5	5.5
23	11	10	10	844	5	5	5
110	11	9.82	10	892	5	5	4.5
185	11	9.5	9.5	946	4	4	4
280	9	9	9	989	4	4	3.75
354	9	8.5	8.5	1041	3.5	3.5	3.5
418	9	8	8	1080	3.5	3.5	3.25
486	9	7.5	7.5	1131	3.5	3	3
589	7	7	7	1211	2.5	2.5	2.5
659	7	6.5	6.5	1285	2	2	2
705	7	6	6				

Table 3.1: Definition of the MPs use to generate the squeeze BP used in 2010.

values at injection, $Q_x = 64.28$, $Q_y = 59.31$, to optimised values with regards to beam-beam interaction, $Q_x = 64.31$, $Q_y = 59.32$.
On figure 3.9b the β function around the IP1 can be seen after and before squeezing to 3.5m. In particular, we observe the significant increase of the maximum in the β function in the triplets, which represents an increase of the transverse beam size of 60%. This increase goes up to 110% when squeezing down to 2m.

Optimisation Based on the experience acquired mainly during the 2010 proton run but also during the ion run, this thesis will present the current status of the squeeze performances and point out issues that have not been noticed during the operation. It is important to keep in mind that the machine was run at a fraction of its capabilities in term of energy, intensity and minimum β^*. Therefore, small issues that can be detected now may have great importance when pushing the performances.
The current squeeze BP takes more than 20 minutes to be executed, during the standard operation, this represents a non negligible part of the turnaround time. As a comparison, the fastest ramp from injection energy to top energy takes 17 minutes. Based on computer simulation and the experimental data provided during the 2010 run, optimised squeeze strategies will be propose for 2011.

Chapter 4

Squeeze performance

4.1 Characterisation

During the design of the machine, several optimization have already been done in order to maximize the performances of the squeeze. However, the behaviour of all the components of the machine were not fully understood. The beams are the first witnesses of the performances of each system, the data acquired during the first year of LHC operation allow to approach the behaviour of the machine from the beam point of view. It is therefore relevant to analyse what has been achieved so far and identify not understood effects that may become relevant for the operation of the next years. Moreover, the understanding of current performances may give leads to follow in order to optimise the squeeze.
As shown on figure 4.1, a lot of work has been achieved during 2010 in order to bring the machine from its commissioning to colliding high energy and high intensity beams. Indeed, before the end of the run with proton, the machine was operated routinely for a few fills with stored energy above 20MJ per beam. It is clear that the machine went through different state before achieving such a performance. There are a significant number of fills during which the machine was used for purposes other than production of collision, that is to say that particular tests and modifications were performed. Thus, the machine was constantly improved, the effect of the different modifications can be seen on various level, and the performance of the machine has greatly evolved. In order to be representative of the performances achieved for production of collision, the analysis of the performance will mainly concern the last weeks of operation with high intensity beams. During this period the state of the machine has remained very stable, that is to say the settings of the all the parameters of the machine have been kept as constant as possible.

4.1.1 β function

As shown by figure 4.2, β_{beat}has been corrected to the level of 20% or below, which is below the tolerance imposed by the collimation system. The measurement was performed with $\beta^* = 2$m at all IPs, similar result is expected with $\beta^* = 3.5$m. The measurement of the β^*s shows (tab. 4.1) that the values achieved corresponds in most cases to the design value of 3.5m. The inaccuracy of the results marked in red is believed to be the result of the measurement technique.

4.1.2 Reproducibility

The fill to fill reproducibility is extremely important for daily operation. Indeed, in a fully reproducible machine, it is possible to transfer correction applied during a fill to the following ones without expecting significantly different results. Even though perfect reproducibility can never be achieved, accelerators based on normal conducting material have shown that a good reproducibility can be achieved. However many

	Beam 1		Beam 2	
	β_x^* [m]	β_y^* [m]	β_x^* [m]	β_y^* [m]
IP1	3.27 ± 0.01	3.8 ± 0.3	3.5 ± 0.2	3.8 ± 0.4
IP2	3.45 ± 0.09	2.6 ± 0.2	3.3 ± 0.3	4.2 ± 0.1
IP5	3.70 ± 2	3.4 ± 0.3	3.7 ± 0.4	3.9 ± 0.4
IP8	3.42 ± 0.14	3.9 ± 0.7	3.6 ± 0.2	3.1 ± 0.5

R. Tomás et al.

Table 4.1: Values of β^* achieved during 2010.

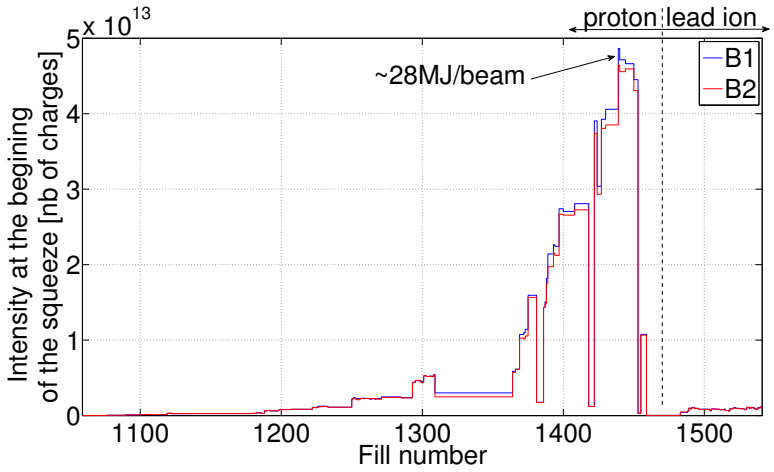

Figure 4.1: Evolution of the intensity of the beams at the beginning of the squeeze. During the last fills with protons an energy exceeding 20MJ per beam was stored in the machine.

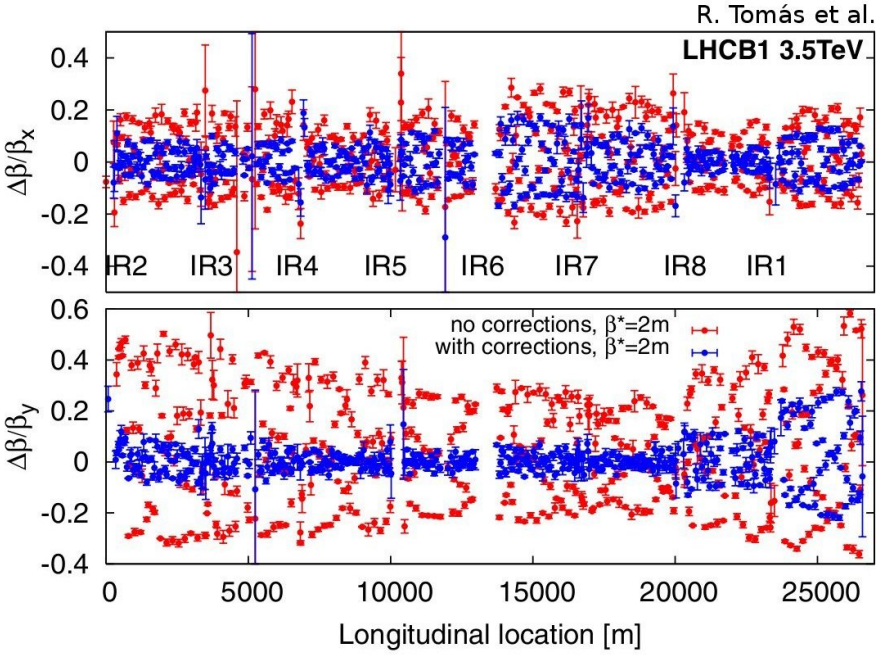

Figure 4.2: Horizontal and vertical β_{beat}measurement with all IPs squeeze down to $\beta^* = 2$m. [16]

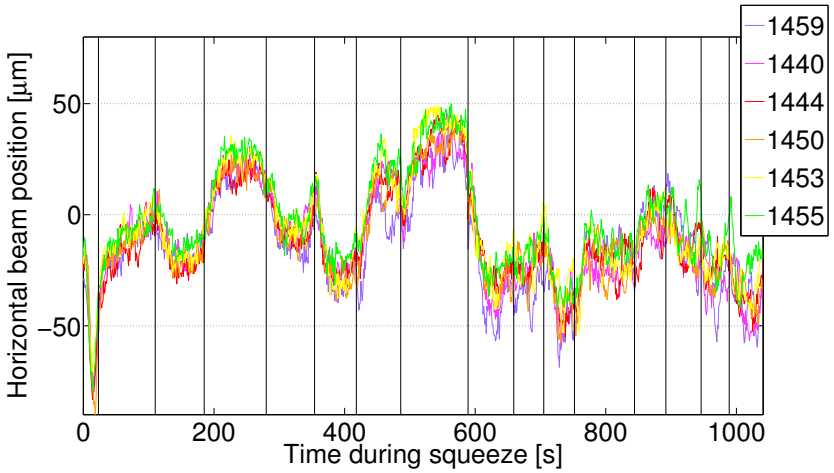

Figure 4.3: Measurement of the beam position at the last BPM before the primary collimators of B1 during a few squeeze performed while operating in stable conditions with high intensities, that is to say with OFB turned on. The curves are shifted with the value at $t = 110$s.

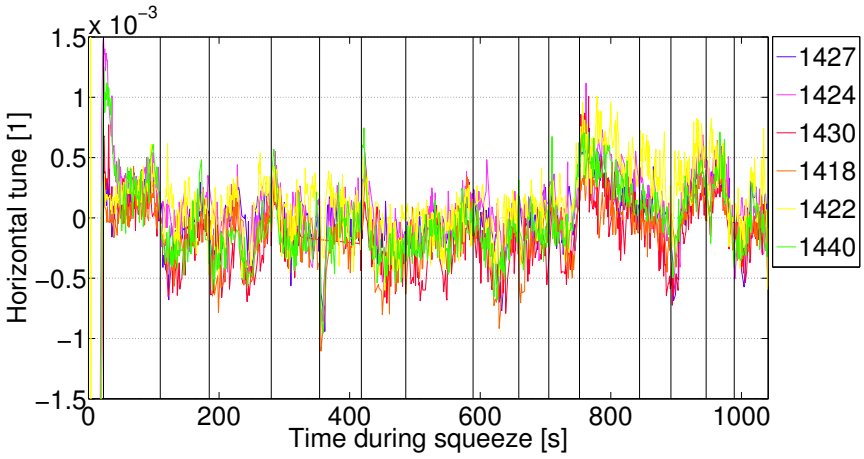

Figure 4.4: Measurement of the tune during a few squeeze performed while operating in stable conditions with high intensities, with QFB turn on. The curves are shifted with the value at $t = 110$s.

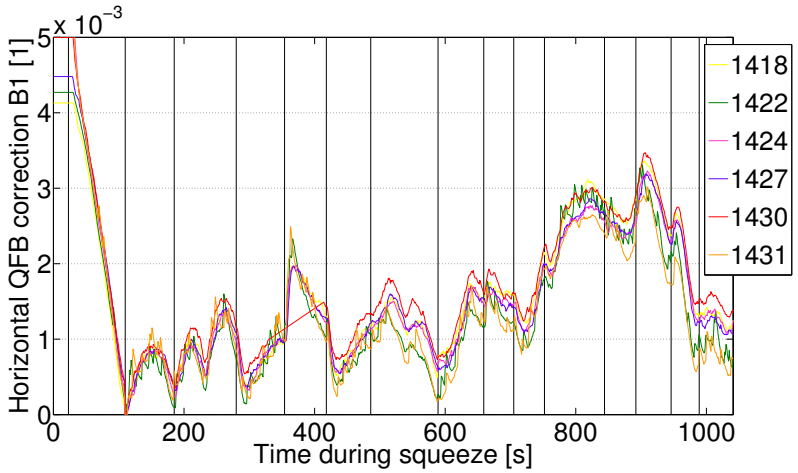

Figure 4.5: Correction provided by the QFB during a few squeeze performed while operating in stable conditions with high intensities. The curves are shifted with the value at $t = 110$s.

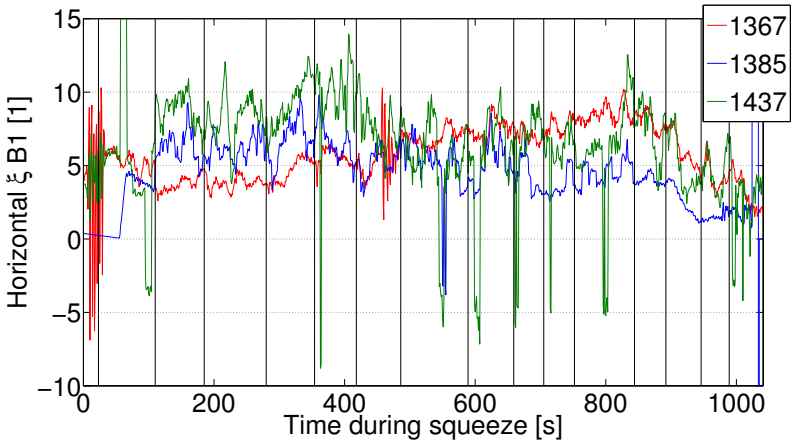

Figure 4.6: Chromaticity measurement as a function of time during the squeeze. All available continuous measurements are shown.

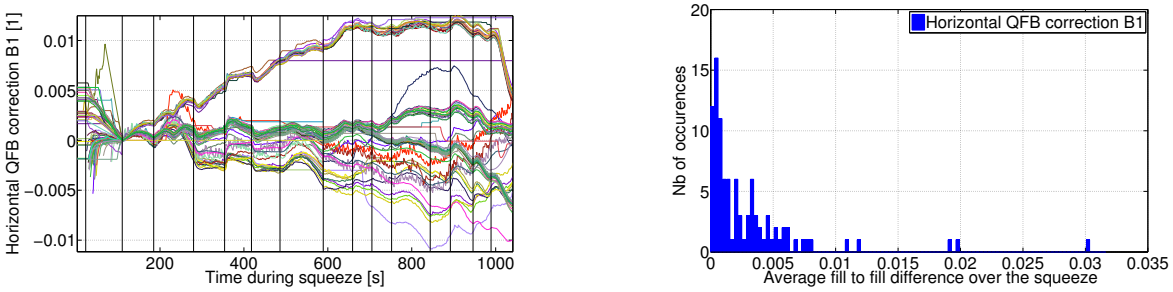

(a) (b)

Figure 4.7: Correction applied by the QFB during each squeeze of the 2010 run with the corresponding distribution of the average of the difference between correction of consecutive fills (δp_i).

concerns arises form the superconducting magnets behaviour encouraging the use of feedback systems on the relevant beam parameters to compensate for lack of reproducibility. The reproducibility η_{r} of a beam parameter p is defined as

$$\eta_{\mathrm{r}} = \sum_{i=1}^{n-1} \frac{\delta p_i}{T}, \ \delta p_i = \int\limits_{\text{squeeze}} |p_{i+1}(t) - p_i(t)| dt \tag{4.1.1}$$

where we have considered the measurement of the parameter $p(t)$ along a squeeze of duration T during n consecutive fills. η_{r} measures the probability of finding a similar behaviour of the parameter p for each execution of the squeeze. Important parameters as a function of time during the squeeze for a subset of fills during stable operation with high intensity beams are shown on figures 4.3, 4.4, 4.5, 4.6 and 4.13. For each parameter, only horizontal plane for beam 1 is shown, however, similar behaviour is observed for the vertical plane and beam 2. In particular, a remarkably good fill to fill reproducibility can be observed for the orbit, tune and coupling. While the QFB is turned on, the tune is maintained at its nominal value within a accuracy of $\sim 10^{-3}$. In these conditions, the reproducibility of the tune can be estimated by considering the correction provided by the QFB. It is important to note that in the case of orbit and tune, the absolute value is different from fill to fill, however the variations from the initial value are identical. To be able to observe properly the reproducibility, the curves have been shifted with the value of the parameter at $t = 110$s. This choice of is motivated by the fact that the QFB was not operational for the first 110s of the squeeze for technical reasons, which explains the abnormal behaviour of the correction provided by the QFB during this period.
The reproducibility of the chromaticity is less evident. Indeed, because of the detrimental effect on the beam dynamics of the energy modulation needed for the measurement, few continuous chromaticity measurement have been performed. However, it is relevant to note that even though the three measurements available are separated by long periods, the variation is not significant, suggesting that the reproducibility of the chromaticity is significantly higher than the one observed with this restricted amount of measurement.

The computation of the reproducibility assumes that the machine is in the same state from one fill to another, which is clearly not the case all along the year. However, in order to take into account only the relevant part of operation, it is interesting to consider an example. The figure 4.7 shows the correction provided by the QFB. Even though many improvements have been made to the machine, we can see that the tune correction is rarely affected significantly. Indeed, we observe large modification between a limited number of fills and an otherwise reproducible behaviour. This behaviour allows to point out fills that do not belong in the computation of the reproducibility, as the fill to fill difference is significantly larger than in normal cases. Thanks to the amount of statistics accumulated along the year, it is easy to isolate the fills that needs to be removed as they appear as non Gaussian elements in the distribution of δp_i (fig. 4.7b). This behaviour of the tune correction is similar to the one of the other beam parameter considered, allowing to compute the values presented in table 4.2 in an identical manner. The reproducibility of linear beam parameters observed during the squeeze is remarkable, the advantage of which will be discussed in section 4.2.

		η_r			
		Beam 1		Beam 2	
		Horizontal	Vertical	Horizontal	Vertical
BPM	$[\mu m]$	8.7 ± 5.2	7.0 ± 4.3	9.6 ± 6.3	8.1 ± 5.4
tune	$[10^{-4}]$	7.7 ± 15.6	6.0 ± 9.2	8.4 ± 15.7	5.9 ± 8.9
QFB	$[10^{-3}]$	2.0 ± 1.9	2.1 ± 1.9	1.4 ± 1.4	1.7 ± 1.6
ξ	[1]	2.7 ± 0.1	1.0 ± 0.3	1.5 ± 0.3	1.2 ± 0.7
$\lvert C^- \rvert$	$[10^{-3}]$	1.8 ± 1.4		1.9 ± 2.2	

Table 4.2: Measurements of reproducibility during standard operation.

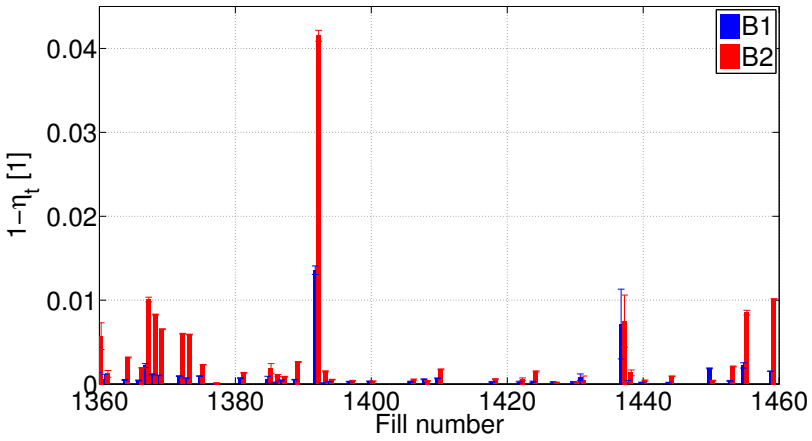

Figure 4.8: Total losses during the squeeze for the last fills of the 2010 proton run with high intensity beams.

4.1.3 Intensity transmission factor

The transmission factor of the squeeze is defined as

$$\eta_t \equiv \frac{I_{\text{After}}}{I_{\text{Before}}} \tag{4.1.2}$$

where I_{Before} and I_{After} refer to the intensity of the beam measured by the BCT at the beginning and at the end of the squeeze. It gives a measure of the total amount of beam lost during the process , $1 - \eta_t$. Figure 4.8 shows $1 - \eta_t$ for both beams as a function of the fill number during stable operation with high intensity beams. Even during stable operation there exists fills that have an extremely bad transmission factor, this is caused by different effect that occur occasionally during operation. As an example, fill 1392 shows abnormally low transmission factor, this fill was dedicated to a purpose different than the production of collision. Such fills are not representative of the average performance of the machine, they are therefore not included in the computation of the average transmission factor. We obtain $1 - \eta_t^{B1} = (3.00 \pm 0.003) \cdot 10^{-3}$ and $1 - \eta_t^{B2} = (15.8 \pm 7) \cdot 10^{-3}$. The striking difference between the two beams is not yet completely understood. Even tough the two beam are designed identically, there are differences in the misalignment and field errors that may cause such a difference in the performance. For both beams the transmission factor is very high, only a small fraction of the beam is lost. However, scaling to the nominal beam, with find that almost 10^{12} proton would be lost, which is equivalent to losing more than a complete bunch. Considering that the beam were squeeze down to 3.5m, which is higher than the nominal value of 0.5m, we can expect that the transmission factor will deteriorate when pushing the squeeze towards the nominal values of β^*. Its is therefore interesting to investigate the processes that led to these losses and possibly correct for it before going to higher intensity and lower β^*.
Nevertheless, as a small fraction of the beam is lost, they do not represent a limitation of the operation. Even when scaling the loss to the one that would be encountered by a nominal beam, the loss are below the quench threshold, therefore they will not cause a dump of the beam (sec. 4.2.2). Moreover, it is important to note that the amount of beam lost during the squeeze is mainly caught by the collimation system, no significant losses are located elsewhere along the ring. This margin suggest that the performances of the squeeze can be improved, notably by reducing the duration of the BP.

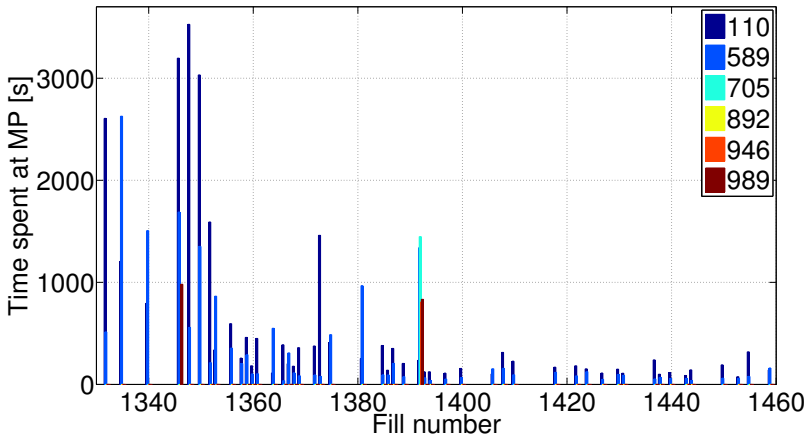

(a) Stable operation with high intensity beams

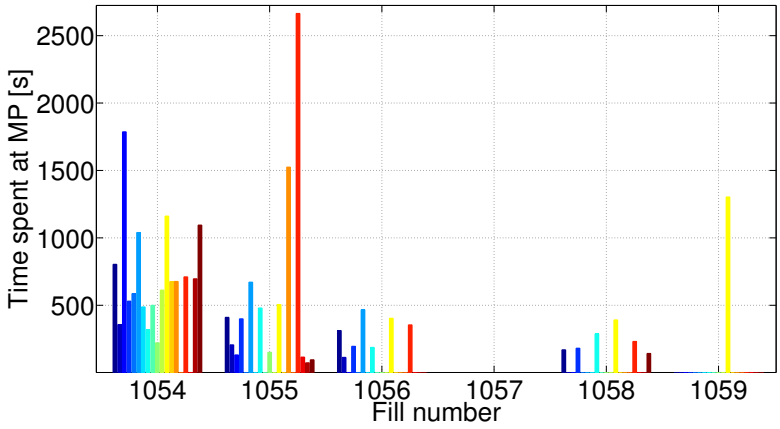

(b) Commissioning

Figure 4.9: Amount of time spend at each MP during the execution of the squeeze. From blue to red, the colours correspond to the different MP listed in table 3.1 in chronological order.

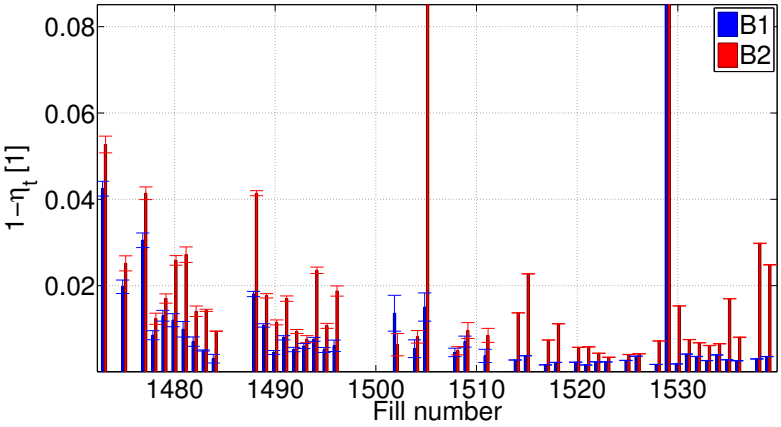

(a) Total loss

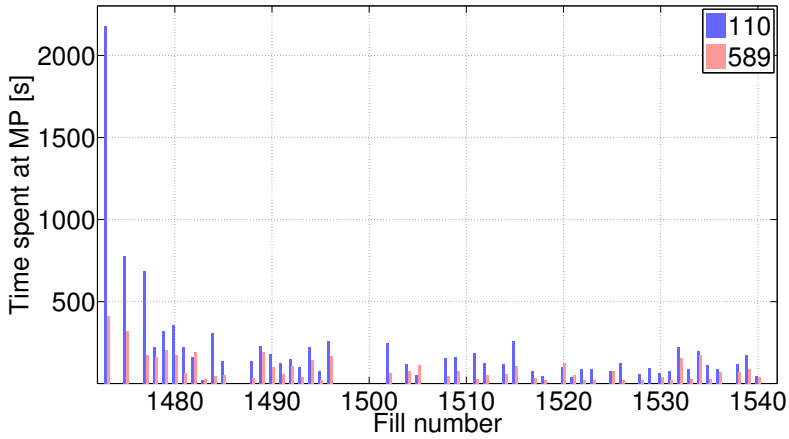

(b) Duration

Figure 4.10: Performance during 2010 heavy ion run.

4.1.4 Duration

The amount of time spend at the MP clearly differ during commissioning and standard operation. During commissioning, a stop at any MP may be needed to perform various measurements, corrections or optimisations. The turnaround time is not a concern at the time of the commissioning. However, the use of all MP is restricted to this period. Indeed, during standard operation, the minimum amount of stop is performed to minimise the duration of the squeeze. As shown by figure 4.9b, each MP has been used to perform a stop, however, the squeeze was ready to be run in only two steps after a few fills. This observation renders questionable the need for a possibility to stop at every MP, therefore justifying a proper analysis of the time that may by saved by using different approaches concerning the MPs (Chap. 5).
During the last fills, two stops were necessary, enhancing the duration of the squeeze of 4 to 5 minutes (fig. 4.9a). This time was required because of the temporary lack of proper implementation of different systems. As the size of the beam is significantly increased at the position of the triplets during the squeeze, the position of the collimators must be changed in order for them to remain the point with smallest aperture. A stop was required during the squeeze to change the position of the collimators, whereas ideally, their position should vary while squeezing, in order to insure the best protection. Moreover, the settings of the OFB needed to be changed to account for a change of crossing angle. The time spend to perform these operations will be saved next year thanks to their automation during the execution of the BP.

4.1.5 Ion run

At the end of the proton run, one month was dedicated to fully stripped lead ion collision at 3.5 TeV per charge. This allowed to run the machine with the same settings as the one used for protons, in order to quickly switch from protons to ions. Only the injection chain is different which imposes a reduction of the intensity. The entire ion run was very stable, no significant changes have been made during operation. Therefore the

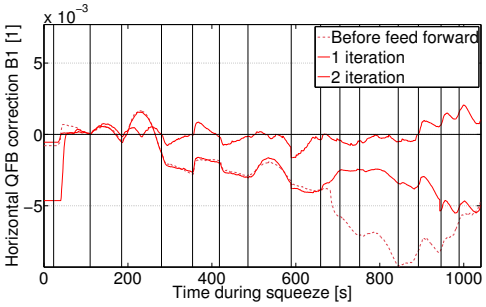

(a) First series of corrections in the Horizontal plane B1

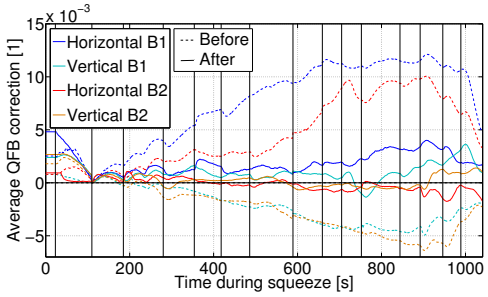

(b) Second series of corrections

Figure 4.11: Average correction provided by the QFB in the horizontal plane of B1 is being reduced thanks to QFF. Similar results are obtained for both plane and both beams.

performances of the ion run are very representative of the status of the squeeze at the end of the year. The results shown on figure 4.10 confirm the ones obtained at the end of the proton run showing that the squeeze can be run in a very stable manner for a long period. Moreover, only a few fills with longer stop at the MPs have been needed, showing that the fast switching from proton to ion was a success, at least with regards to the squeeze.

4.2 Optimisation

4.2.1 Feed-forward

Feedback systems have been introduced to keep under control critical beam parameters. Even though the reproducibility would be good enough to do without them during the squeeze, they ease the operation, as the corrections are automatized. Moreover, it has been shown that even though the average reproducibility is good, there exist exceptions when large differences are observed between consecutive fills, the feedback systems therefore improve the operational efficiency. However, the feedback systems are not perfect, failures are observed occasionally due to either hardware or beam issue. Whereas the first option is very rare, the second is commonly observed for the QFB. For example, the current QFB is automatically shut down when high coupling is detected, as its proper operation is compromised. By keeping the correction provided by the QFB minimal, the chance of observing large deviations of the tune in case of QFB failure are reduced. In order to keep the corrections minimal, it is possible to introduce a feed-forward procedure in which the corrections of the preceding squeeze, or an average over preceding squeezes, are stored in the BP, such that they are automatically played during the following fills, therefore relieving the QFB.
Three iterations of feed-forward based on the average correction over a few fills have been done during the 2010 proton run, clearly visible on figures 4.11. After a few iteration, the tune correction can be maintained within a range of $5 \cdot 10^{-3}$. A failure of the QFB would not be critical for the operation in such conditions. Based on the number of iteration needed to obtain a reasonable correction and the general reproducibility, the implementation of an automatic feed-forward may be superfluous, however performing a feed-forward regularly can improve the operational efficiency.

Chromaticity For the moment, there is no chromaticity feedback system, because of the detrimental effect of the measurement technique. However, the continuous measurement over a few fill have shown that reproducibility is sufficient to perform a feed-forward based on the average over a few measurements. Not enough chromaticity measurement have been performed during 2010 to perform a proper feed-forward. However, the three continuous measurements have been performed at long interval, ~ 100 fills, therefore the chromaticity has not been subject to significant variation during the year. It would be relevant to perform a series of continuous chromaticity measurement at the beginning of next year, while the intensity of the beams is the lowest. This would allow to feed-forward the appropriate correction and therefore obtain a chromaticity closer to the nominal one along the squeeze BP.

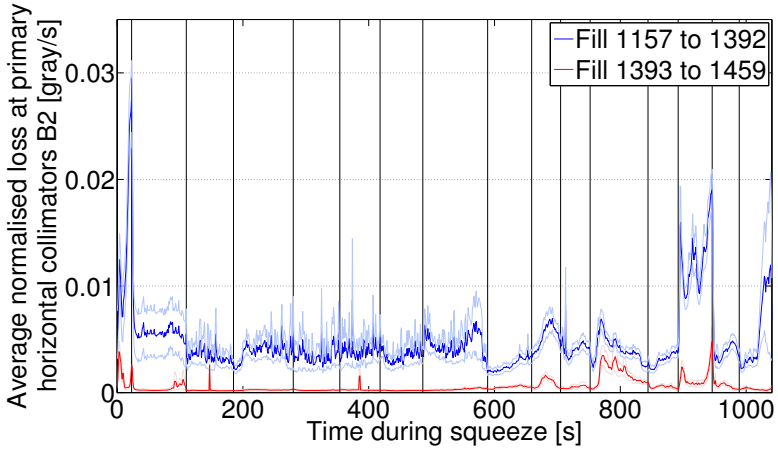

(a) Losses

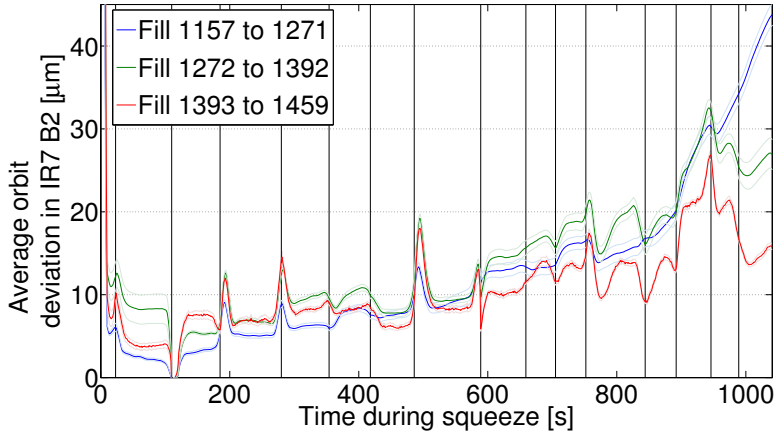

(b) Orbit

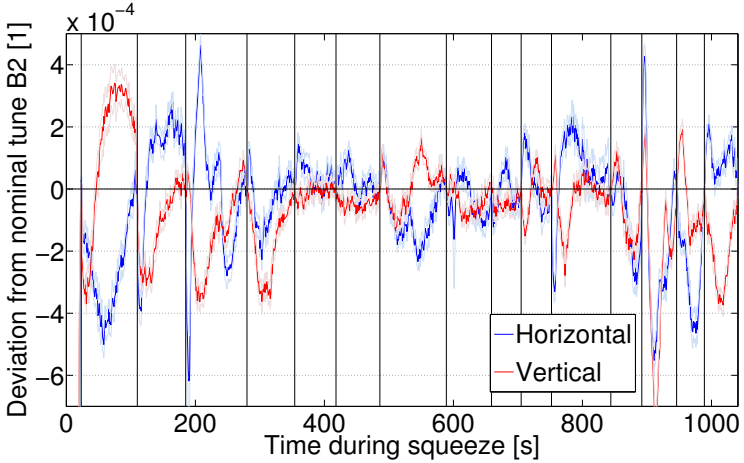

(c) Tune

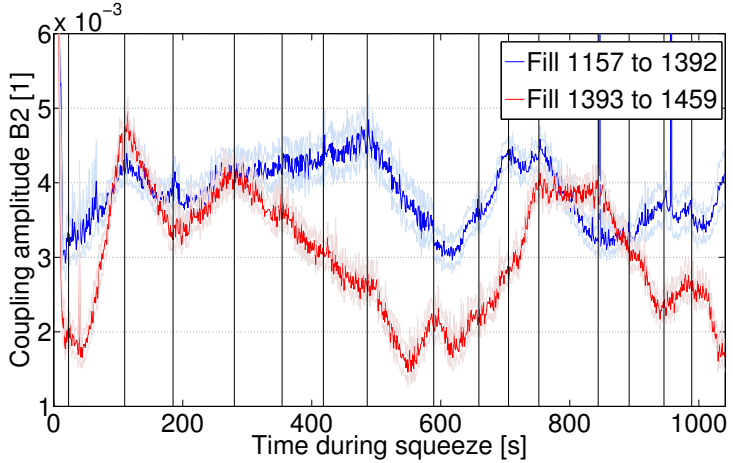

(d) Coupling

Figure 4.12: Average losses, orbit, tune and coupling amplitude over a period from the commissioning of the QFB (fill 1157) to the end of the run with proton (fill 1459). The averages are split in parts when significant changes occurred. Since fill 1272, the orbit is significantly optimized and a coupling correction was applied during fill 1393.

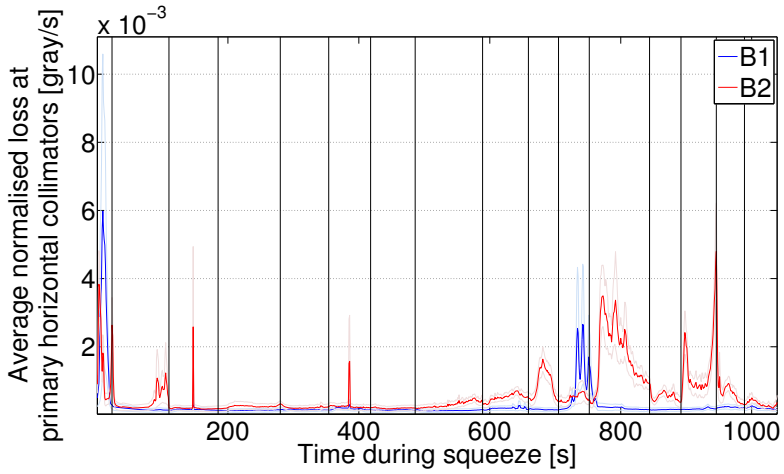

Figure 4.13: Losses detected at the primary horizontal collimator, normalized with the beam intensity at the beginning of the squeeze and scaled to the nominal intensity.

4.2.2 Systematic losses

In order to discover the nature of the small amount of beam lost during the squeeze, a precise measurement of the intensity of the beam is required. However, the variation of intensity expected from the measurement of the transmission factor are in the order of 1%, therefore the resolution of the BCT is not sufficient for a precise analysis of the losses, the BLM system offers another approach. As they measure the radioactivity outside the beam pipe, they do not allow one to measure the variation of intensity but they provide the distribution of losses both in position along the ring and time during the squeeze. The collimators have been designed to catch particles performing anomalous betatron motion before they are lost some place else in the machine, the losses at the primary collimators are therefore orders of magnitude higher than the one that occur along the ring, they are therefore very representative of the total amount losses.

The intensity of the beams is different from fill to fill. As the radioactivity measured by the BLM is linearly dependent on the intensity of the beams, it is normalised with the intensity of the beam at the beginning of the squeeze, such that the resulting measure is comparable from fill to fill. To recover more apprehensible values, the measurements are scaled to the nominal intensity. As can be seen on figures 4.13, the losses observed at the primary horizontal collimators have a systematic component. There are critical times at which loss spikes are systematically observed. A similar behaviour is also present in both vertical and skew plans, however the amplitude of the losses are significantly lower. Moreover, the losses are simultaneous in all plans. Even though the maximum losses observed are way below the beam dump threshold, it is interesting to understand their nature, for they may become relevant in a near future.

Orbit Plot 4.12b shows the average over all BPM in the betatron cleaning insertion of the absolute value of the orbit deviation from its value at $t = 110$s. There are orbit spikes systematically appearing at the MPs or a few seconds after. The one at $t = 750$s is correlated with a significant increase of losses. However, the orbit deviation is not the only cause of loss as they continue even after the orbit has returned to its original value. Losses between $t = 898$s and $t = 950$s are also correlated with a globally higher orbit deviation. The one to one correlation between the orbit drifts and losses cannot be established, because such small variation of the orbit should cause significant losses only if they occur at the position of the collimator jaw. By considering fill 1439 as an example, on figure 4.14 which shows the position measured at the BPM closest to the primary collimators. This confirms that there are orbit distortions at the primary collimators. However, the correlation with the losses still is imperfect, pointing out that the orbit deviations themselves cannot fully explain the losses observed.

A second important feature of the orbit measurement is the slow drift to $\sim 20\mu$m which is not understood.

Tune The losses during the first step are caused by the crossing of tune resonances while moving from injection tunes to collision tunes. These losses are unavoidable, however they can be minimized by choosing to change the tune when the available aperture is maximum, which is before the squeeze.

Similarly to the orbit, abrupt tune drift are observed at the MPs or a few seconds after. The amplitude and time scale of the tune drifts correspond to the one observed in 5.2, due to the mistreatment of hysteresis. Indeed, the changes are faster that the QFB reaction time, therefore there are still visible while it is on. The

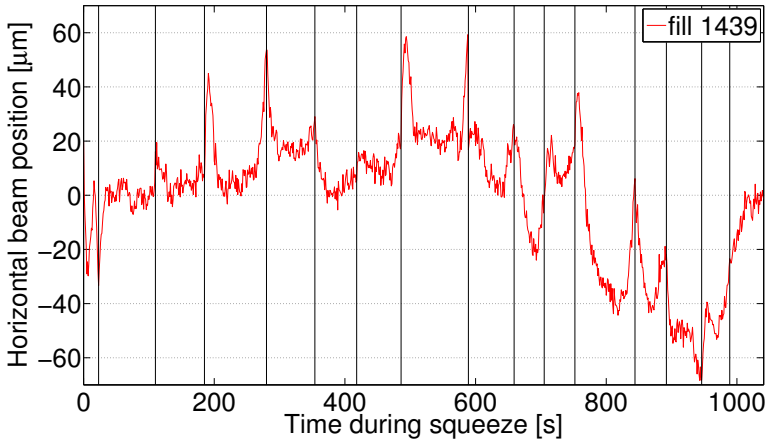

Figure 4.14: Horizontal orbit measured by the BPM closest to the primary collimator of B2, which is located 18m downstream.

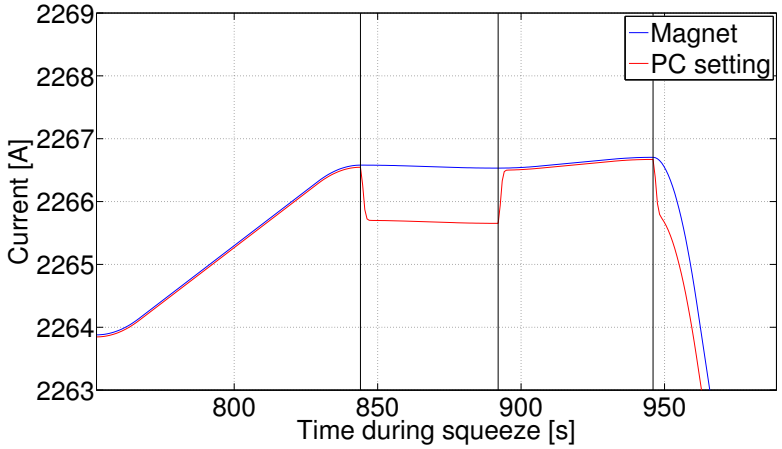

Figure 4.15: Design current in a quadrupole located in a matching section, compared to the instruction given to the PC that takes into account the hysteresis of the magnet.

orbit spikes observed are clearly correlated with the fast changes of tune. Moreover, the interval between $t = 898$s and $t = 950$s is also more critical from the point of view of the tune.

The source of the fast orbit and tune changes must come from a fast change of settings, such that the feedback systems are not able to follow, that is to say within a time scale of the second. The slow deviation that can be seen on the tune may be caused by different process. Two hypothesis are proposed to explain both effects.

Coupling The figure 4.12d shows the coupling correction that has been made during fill 1392. Figure 4.12a shows a significant difference before and after this correction, the total dose measured at the primary collimator is greatly diminished. Indeed, globally the coupling has been lowered, therefore lowering the total amount of beam lost. However, in the most critical interval, the coupling was not significantly improved, leading nevertheless to a lowering of the losses in this region. This effect is not yet fully understood.

As the coupling is currently way higher than the design value ($|C^-| \ll 10^{-3}$), there is no doubt that an improvement of the coupling correction has to be made. It is important to keep in mind, however, that the coupling measurement is not fully reliable in case of low signal to noise ratio, which was often the case during 2010 operation, especially when working with high intensity. The algorithms used to filter out the noise have been subject to modifications during the year. The coupling may have been globally overestimated, which does not modify the previous conclusion.

Hysteresis The effect of a hypothetical mistreatment of hysteresis on the tune is demonstrated with the simulation of BP (sec. 5.2). Its effect is visible while running with the QFB turned on, as the changes of hysteresis branch happen faster than the response time of the feedback system.
Whereas the orbit is not concerned by the strength of the quadrupole in a perfect machine, it become relevant when introducing misalignments. The computation of the effect of the hysteresis on the orbit can not be performed without the knowledge of the misalignment of the quadrupoles. However, few magnets are concerned by hysteresis at each IP, therefore the order of magnitude of the orbit distortion generated by the fake hysteresis can be guessed by introducing the kick due to the change of strength of one typical matching quadrupole ($L \sim 5\text{m}, k \sim 5 \cdot 10^{-4}\text{T/m}, \Delta k \sim 10^{-7}\text{T/m}$) with the tolerated misalignment of the quadrupole $\delta_x \sim 1.5\mu m$ computed with equ.2.9.1 into equ.2.9.2.

$$x = \frac{e \cdot L}{k\delta_x} \cdot \frac{\sqrt{\beta(s) \cdot \beta(s_0)}}{2\sin(\pi Q)} \cos\left(\phi(s) - \pi Q\right) \tag{4.2.1}$$

Differentiating, introducing the numerical value reasonably assuming $\beta(s) = \beta(s_0) \sim 300\text{m}$ and choosing the cosine such as maximizing the orbit distortion.

$$\Delta x = \frac{e \cdot L}{k^2\delta_x} \Delta k \cdot \frac{\sqrt{\beta(s) \cdot \beta(s_0)}}{2\sin(\pi Q)} \sim 6\mu m \tag{4.2.2}$$

This value is overestimated, however, a few magnets are concerned by hysteresis at each MP. The order of magnitude correspond to the orbit distortions observed at the MPs, the orbit distortions may therefore be explained by the mistreatment of hysteresis.

The systematic losses observed during the squeeze are not yet completely understood, however both orbit and tune measurement suggest that the fast change of current in the magnet introduced to account for the change of hysteresis branch (fig. 4.15) is responsible for part of it. The model introduced assume a two branches hysteresis diagram, which correspond to the hysteresis of a normal conducting ferromagnetic material, like the iron yoke. However the contribution from the superconducting coils follow a four branch hysteresis diagram, poorly approximated in the current model. Moreover, the calibration branches have been measured when ramping up and down to the saturation field, whereas the change of derivative encountered during operation happen far from the saturation values, the correct behaviour of the field is not properly modelled.
The treatment of hysteresis may be incorrect for only a subset of quadrupole. The lack of knowledge about misalignments has only allowed a qualitative validation of this hypothesis with the orbit measurement. However, the simulation of tune including fake change of hysteresis branch allows a quantitative analysis (sec. 5.2). A remarkable agreement between measurements and simulation is shown when including into the simulation the fake changes of hysteresis branch of all quadrupoles except the correctors, for which the hysteresis is not taken into account. This suggest that the treatment of hysteresis is incorrect for all the quadrupoles and therefore should be modified.

The development and implementation of a more accurate model of the change of hysteresis branch will require a significant amount of work. However, a simplified model may be sufficient. Indeed, the real effect of the change of hysteresis branch is expected to be much less detrimental to the operation than the fake change that have been introduced during 2010 for two reasons. Firstly, the amplitude of the change of strength was computed from the measurement of up and down ramping from one saturation value to the other, which is the maximum amplitude, the real amplitude can only be smaller. Secondly, the change of hysteresis branch was performed as fast as possible, taking into account the maximum current rate and acceleration that can be provided by the PC. The previous results suggest that the real time scale of this change is slower, the consequences on the beam parameters may therefore be within the time response of the feedback systems. Therefore the complete removal of the treatment of hysteresis from the generation process will have less consequences from the beam dynamics point of view. This approach is also motivated by the vanishing effect of hysteresis while increasing the current in the magnets, therefore while increasing the beam energy.

Chapter 5

Simulation of beam process

It has been shown (fig. 4.9b) that the commissioning of the squeeze can take a few fills, this time needs to be spent every time a new β^* configuration is introduced. As the time is extremely precious during the commissioning, because numerous other beam studies and the production of collision require a lot of time, it is necessary to be able to test new propositions for optimisation, in order to apply them in the shortest time span, avoiding the waste of precious machine time. In a similar manner, the introduction of any newly generated BP can benefit from a check before effectively being run by the machine.

5.1 Simulation

The Methodical Accelerator Design X (MADX) [17] program is used to compute the behaviour of linear beam parameters during the squeeze BP based on the strengths of the magnets. The position and length of the magnets are defined based on the latest measurements, however neither misalignment nor field errors are included. An accurate model of these errors is not yet available.
The strength of each magnet as a function of time is extracted from the control system. They have been computed based on the interpolation of the settings in between the MPs including a round off at each MP that account for each magnet's limitations in current derivatives. It is important to note that the strengths considered in the simulation are the ones used to compute the current that needs to be provided by the PCs based on the knowledge of the transfer function of each magnet, which includes, for example, the modelling of hysteresis and lower/higher field error. These effects are therefore not included in the simulation.
Such simulation of a perfect machine provide an estimation of the error due to the introduction of settings that are not perfectly matched, based on the assumption that the machine do not deviate too much from the perfect one. In the real machine, the error introduced by the unmatched settings may not be the principle cause of error. As we are considering linear beam parameters, the error estimated by the simulation adds up with the one arising from other sources. In case of large error caused by other systems, the error estimated may be masked by other sources.
Simulation of relevant beam parameters during the squeeze BP used for standard operation in 2010 are shown in figure 5.1.

5.2 Validation

In the perfect machine approximation, only the optic is changed during the squeeze, therefore only strength of the quadrupoles and higher order magnets are being varied. A variation of the orbit can arise from the off-centred orbit in the triplet, in case of a crossing angle is introduced, which is not considered here. No orbit variations are expected from the simulation. Moreover, neither skew elements nor solenoid fields are included in the simulation, thus no coupling is expected. Therefore, the main interests of the simulation are tune, chromaticity and β_{beat}.

5.2.1 Tune

To consider the tune measurements, it is important to separate the time before and after the commissioning of the QFB. Indeed, the error introduced by the unmatched settings can be seen when the QFB is off, but when turned on, the QFB will compensate for the errors to maintain the tune at its nominal value. Therefore the measurements cannot correspond to the values given by the simulation. Data collected before the QFB are therefore used for the validation.

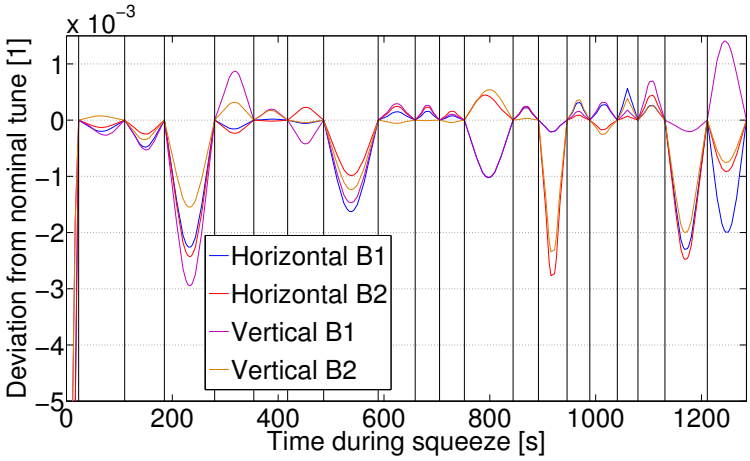

(a) Tune

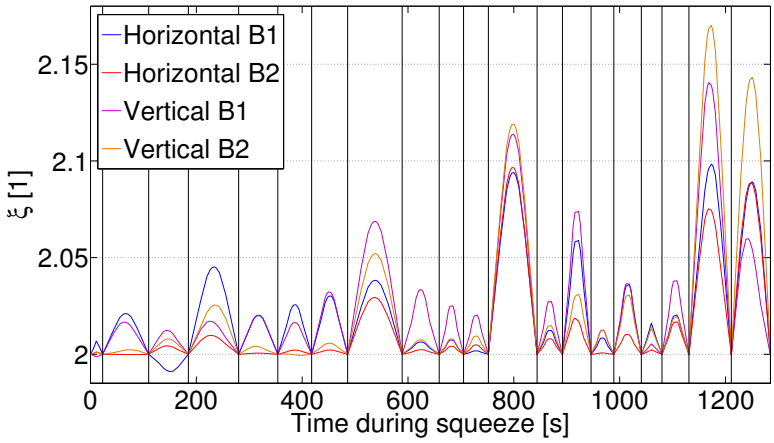

(b) Chromaticity

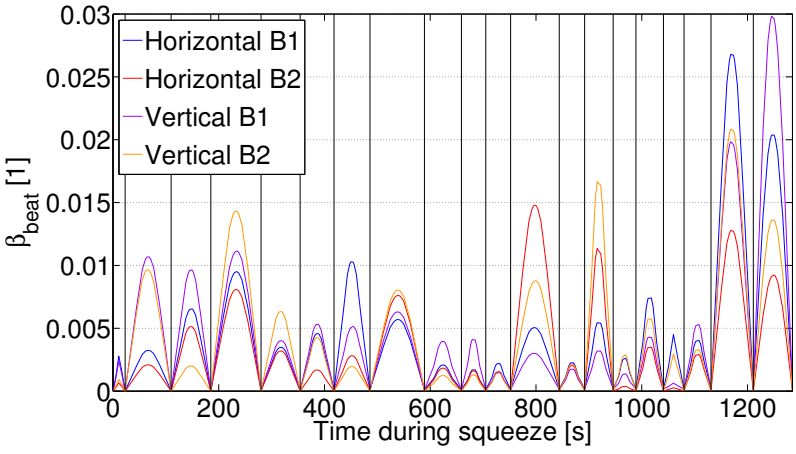

(c) β_{beat}

Figure 5.1: MADX simulation based on the settings of each magnet during the squeeze BP used for standard operation in 2010.

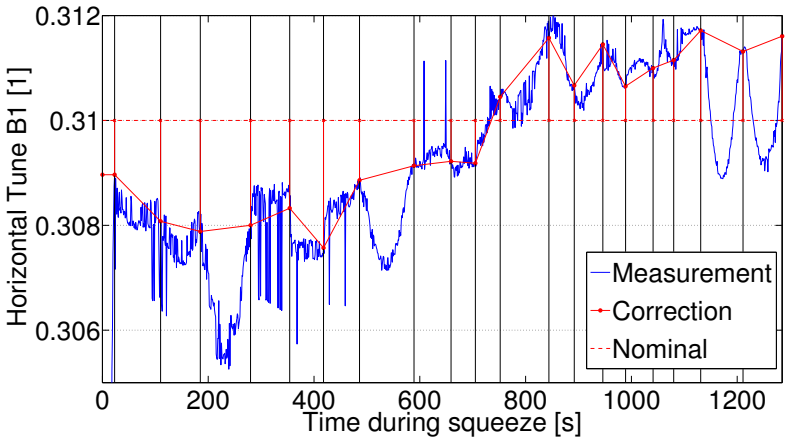

Figure 5.2: Example of untouched tune measurement.

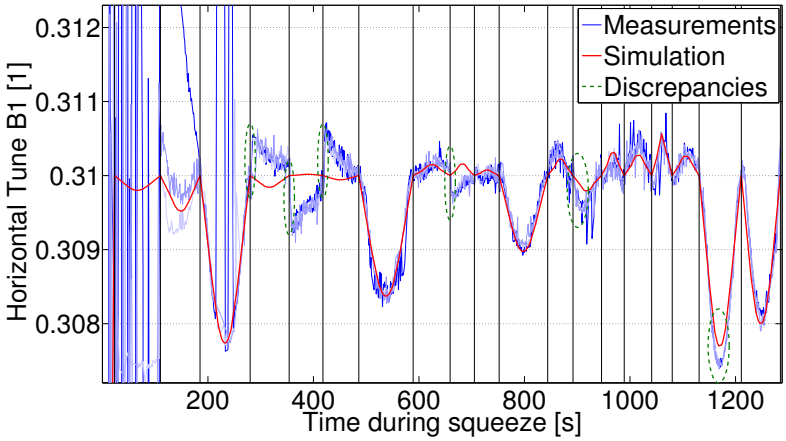

Figure 5.3: Corrected tune measurement compared with simulation

		Average difference $[10^{-4}]$	
		B1	B2
Tune	Horizontal	1.36	5.56
	Vertical	3.80	2.49

Table 5.1: Average difference between tune measurement and simulation.

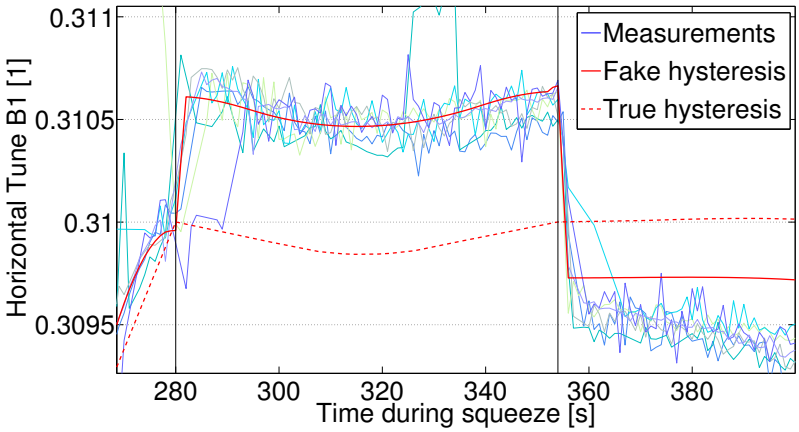

Figure 5.4: Comparison of tune measurement with simulation including fake changes of hysteresis branch.

In order to compare the simulation with measurements, it is necessary to treat them so that they fit the frame of the simulation. Indeed, the simulations being based on the perfect machine, each parameter is equal to its nominal value at the MPs and vary in between because of the unmatched settings. However, figure 5.2 shows that the measured tune is different from the nominal one at the MPs due to numerous other source of error. The most important error is in this case voluntary. During the commissioning, the operators can choose to keep certain parameters different from the nominal ones. In the case of tune, it was chosen to keep it lower than nominal at the beginning of the squeeze in order to keep away from the third order resonance $Q_x = 64 + \frac{1}{3}$. Assuming that the error due to the unmatched optics adds on top of the error caused by other sources, it is possible to discard them by subtracting the background, therefore isolating the error of interest. An example of such correction is shown on figure 5.2. By systematically applying this correction and averaging over a few fills, we obtain the result of figure 5.3, the simulation and measurements are then comparable.
The spikes of constants amplitude in the tune measurement are not physical, they result from the measurement process. The tune spectrum is composed of several peaks, the tune measurement is based on the detection of peak with highest amplitude. In certain conditions other spikes can momentarily be higher that the tune spikes, which causes the jump seen in the tune measurement. A proper filter is applied to remove non physical points from the measurement, the first hundreds of seconds of figure 5.3 shows that the filter is not sufficient in certain cases, in particular when the rate of the spike is too high, revealing a too low signal to noise ratio in the tune spectrum.
Even though the simulation is in general very accurate when discarding the high noise region, some discrepancies are observed. Similar results can be found for both beam and both planes. The average difference between measurement and simulation excluding the regions with discrepancies are summarized in table 5.1.

Hysteresis As discussed in section 4.2.2, the current treatment of hysteresis is highly suspicious. The discrepancies between simulation and measurement have some feature that matches the hypothesis of an inappropriate hysteresis treatment. Indeed, the time scale of the discrepancies observed is in the order of the second, which correspond to the current time scale of change of hysteresis branch. Moreover, the change of sign of the time derivative of the current can only occur at the MP, as the settings are interpolated linearly in between, which is when all the discrepancies except the last one are observed. In order to check this hypothesis, the settings of the magnets concerned by hysteresis were modified in the simulation, assuming that the changes of hysteresis branch that are introduced during the generation are not physical. Practically, the strength of the magnetic field felt by the beam is no longer the one defined by the strength only, the magnetic field generated by the current added to change hysteresis branch has to be added on top of it. If this interpretation is correct, the correction of the tune applied to keep only the error arising from the unmatched optics is no longer valid. Indeed, the introduction of hysteresis in the simulation modifies the

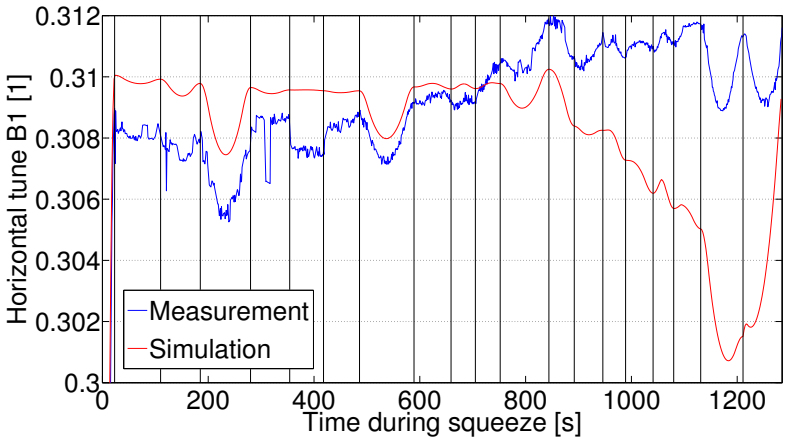

Figure 5.5: Simulation of the tune with corrections included perturbatively.

value of the beam parameters at the MPs. Moreover, the simulation do not concern a perfect machine any more, but a machine containing only one source of error. In these conditions, it is harder to obtain comparable measurements and simulation. However, it is possible to compare the amplitude of the fast tune jump observed in the measurement and simulation as it does not depend on the value of tune at the MPs and the other sources of error are way slower than the one expected from the fake change of hysteresis branch. Focusing around $t = 300$s, where the biggest discrepancy is observed and removing the correction of the tune at the points $t = 354$s and $t = 418$s, figure 5.4 shows the remarkably good agreement of measurements and simulation around the first MP.
This observation not only validates the simulation from the point of view of the tune, but also gives an evidence that the implementation of the modelling of the hysteresis is not accurate. The consequence of this inaccuracy is discussed in 4.2.2.

5.2.2 Chromaticity and $\beta_{\mathbf{beat}}$

Whereas the nominal chromaticity is 2 units in both planes, fig. 4.6 shows that the measured one varies greatly between 2 and 10 units dring the squeeze. Moreover, only three continuous measurement of the chromaticity have been performed, excluding the possibility to have some statistics. In the case of β_{beat}, few measurements have been made [18], showing variation in the range of 5%. Therefore, the error estimated by the simulation, figures 5.1, are clearly under the detection level of the current measurement in both cases. Indeed, the errors are dominated by other sources.
The good accuracy of the simulation observed with the tune estimates suggests that they are reliable to compute the error introduced by the unmatched settings between the MPs. Even though a proper validation could not be performed with the available measurements, the simulation of chromaticity and β_{beat}will be assumed to be accurate in a frame identical to the tune simulation. That is to say that the error estimated by the simulation adds on top of the existing error caused by other sources.

5.3 Operational efficiency during commissioning

The frame of the simulation may be extended by considering a perturbative approach. Considering that the machine is fully corrected at the beginning of the BP, the variation of the strength of each magnet, including the correctors, are included as a perturbation of the perfect machine. The effect of other sources of error, such as the correction provided by the operators, is thus introduced in the simulation.
Such a simulation is motivated by the improvement of operational efficiency that it can provide, especially during the commissioning phase. Indeed, during this phase, corrections are introduce manually in the BP by the means of the different knobs to compensate the observed deviation of the beam parameters with respect to their nominal values. Experience has shown that small errors during this procedure can lead to a dump of the beam. The simulations could, in principle, be used to check the validity of the settings before they are actually performed by the machine, limiting the risk of a beam dump due to human factor.
This method can be used in a very limited extend. Indeed, some corrector magnets strength vary strongly along the squeeze, compromising the perturbative approach. An example can be observed on figure 5.5, clearly showing that this method cannot be used to an extend sufficient for daily operation.

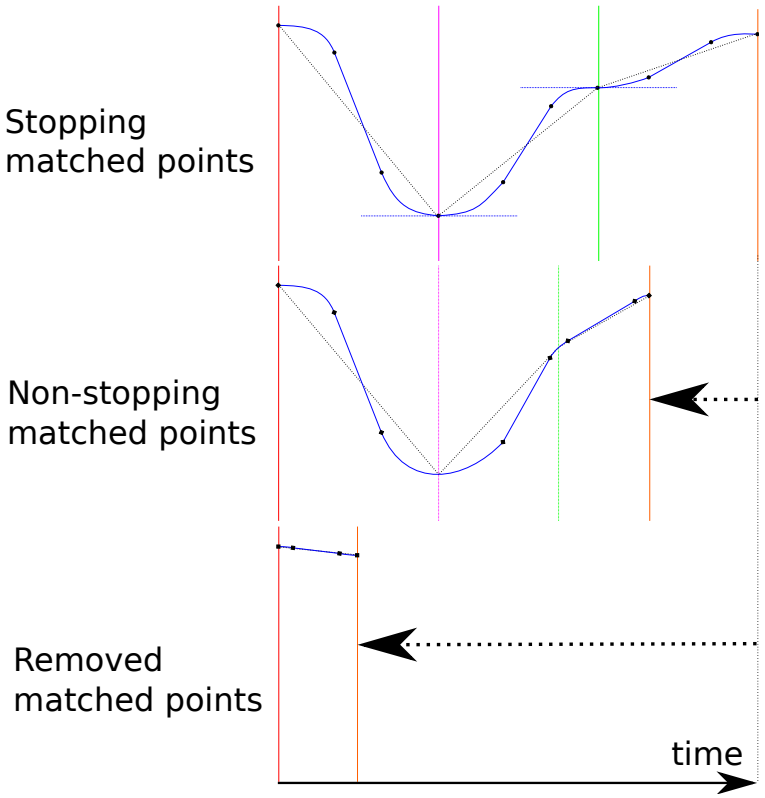

Figure 5.6: Schematics of the settings of a hypothetical parameter using different optimisation strategy to reduce the duration of the squeeze. The dashed arrows represents the time that may be saved in this particular case.

5.4 Optimisation of the squeeze duration

5.4.1 Run configurations

β^* configuration Input from the experiments remain needed in order to determine the squeeze configuration of 2011. While running with protons, CMS and ATLAS both require the highest luminosity achievable, whereas ALICE and LHCb demands may be lower. The requirements are also different for ion operation, moreover, they may vary from year to year according to the needs of the detectors. It is also relevant to note that an optimised BP that increases the β^* at IP5 to fill the requirements of the Total Elastic and diffractive cross section Measurement (TOTEM) experiment is also foreseen. Therefore, new optimised strategies will have to be determined as the demands changes, two study cases are presented in order to characterise different means for optimisation. The first study case corresponds to the strategy chosen for 2010 in which all IPs are squeezed down to 2m, the second is a likely scenario for 2011, only CMS and ATLAS are squeezed down to 0.8m and LHCb to 5m keeping ALICE untouched. It is important to note that squeezing down to 0.8m is highly unlikely, the squeeze will most likely be executed down to 1.5m.

Energy The optic function computed in the simulation is based on the strength of the magnets that is independent on the energy of the beam, the resulting beam parameters are therefore independent as well. On the other hand, the current of the magnet corresponding to a certain strength depends on the energy of the beam. The generation of BP therefore depends of the energy of the beam. In particular, the duration of each interval between the MPs will be increased.
The energy of the beam that will be used for operation in 2011 is still to be decided. As the value of 2010 is likely to be kept, the following study considers BPs generated for operation with 3.5TeV beams. In case the energy is modified, the position of the MPs will be different, but the result of the simulation will not be affected.

5.4.2 Optimisation methods

Two different approaches can be taken to minimize the duration of the squeeze. Either MPs can be completely removed or the ability to stop at them may be abandoned. The figure 5.6 represents the difference in the

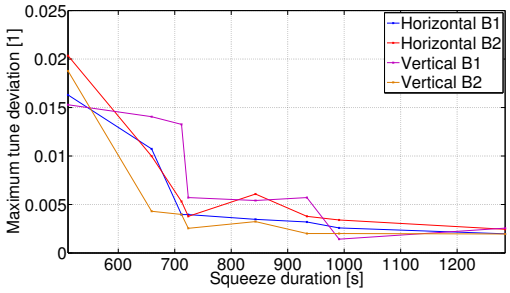

(a) Tune

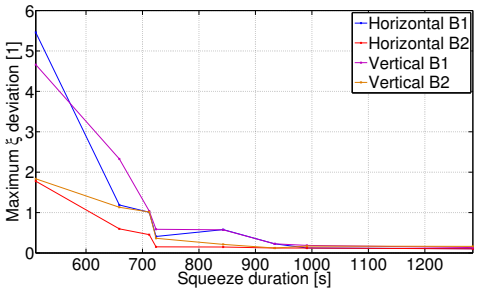

(b) Chromaticity

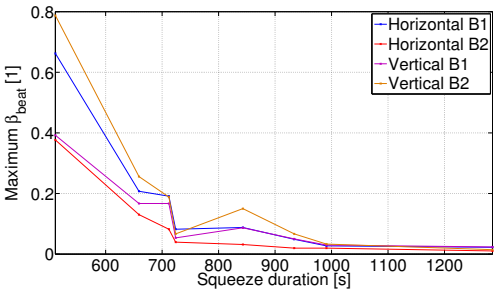

(c) β_{beat}

Figure 5.7: Maximum deviation expected from the simulation for BPs of different duration. All IPs are squeezed to 2m.

strategies from the point of view of the settings of a hypothetical magnet.
No assumption can be made on the behaviour of all the settings during the squeeze. Indeed, whereas the strengths of the triplets of each IP follow monotone functions, there exists magnets, typically in the matching sections, that perform more complex functions in time.
In the schematics 5.6, we see that for fixed MPs at the beginning and at the end, removing the intermediate ones clearly is the most efficient method from the point of view of timing. However, it also introduces the largest deviation from the nominal settings, possibly leading to large variation in the beam parameters. The non-stopping MP approach allows to make smaller savings in time, but the deviations expected from the beam parameters are not significantly larger than the one expected with the current method. The following sections aim to find the best compromise between the different approaches based on the simulation introduced before.

5.4.3 Number of matched points

Removing MPs leads to variations of the beam parameters that can exceed the tolerances. For the first year of operation, the number of MP was chosen to minimise the error arising from the mismatched optics. As the experience of 2010 showed that the different beam parameters were well under control during the squeeze, it may be possible to remove some of the MPs and still be able to correct the error introduced. A shorter BP can therefore be used if the beam parameters variation in between the MPs can be handled by the specific correcting scheme if it exists and if it is within the tolerances otherwise. Considering the configuration of 2010, figures 5.7 shows the maximum deviation expected from the simulation for BPs of shorter duration for different beam parameters. Whereas the tune and chromaticity variations can be compensated by the specific correction scheme even for the shortest BP, $\beta_{\text{beat}}$is more critical. Indeed, no continuous β_{beat}correction is available yet and the tolerances are tight. As discussed in 2.8, the collimation system heavily rely on the knowledge of the β function at the position of the collimator jaws, the β_{beat}must therefore be kept below 20%.
It is important to keep in mind that this dynamic $\beta_{\text{beat}}$is added on top of the static one already present due to field errors and misalignments. Assuming that the latter can be corrected up to 10% [16] and considering figure 5.7c, durations below 714s are excluded for squeezing all IPs to 2m. With such a BP, almost 10 minutes may be saved compared to the BP used during 2010 operation. However, the estimated total $\beta_{\text{beat}}$is close to the tolerance. A BP of duration 991s offers a more secure approach, as the deviations expected are not significantly higher than the current ones still gaining 5 minutes.
Similar observations can be made when considering the configuration of 2011. Based on figures 5.8a to

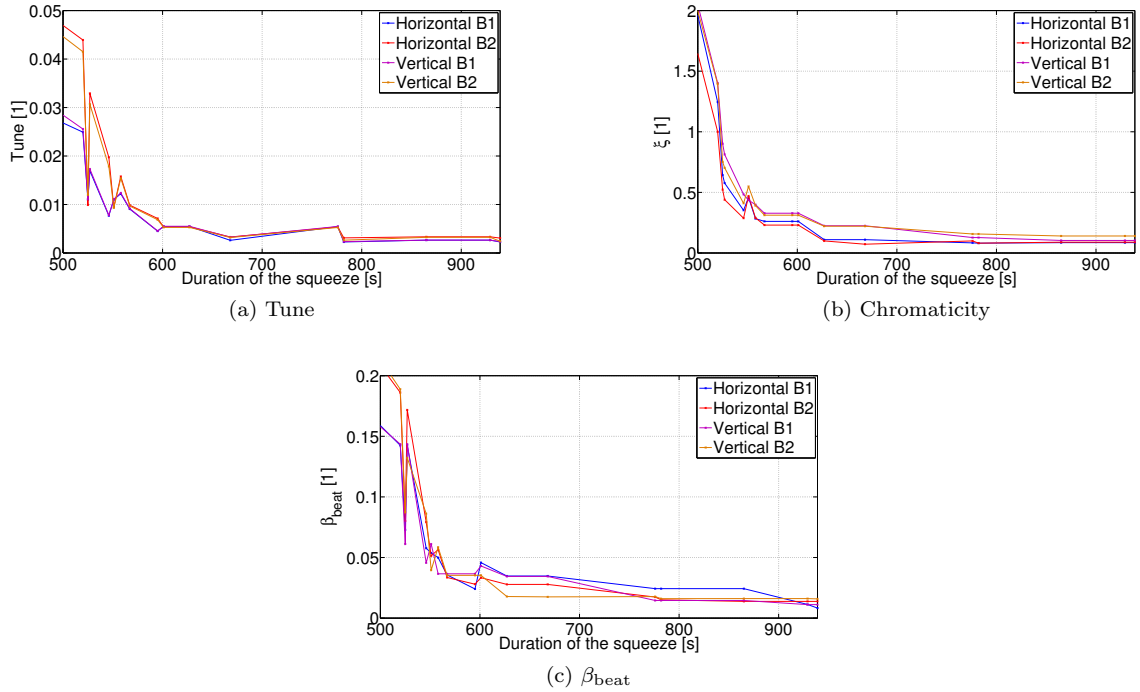

(a) Tune

(b) Chromaticity

(c) β_{beat}

Figure 5.8: Maximum deviation expected from the simulation for BPs of different duration. IP1 and IP5 are squeezed down to 0.8m, whereas IP8 is squeezed down to 5m, IP2 is not squeezed. The maximum deviation is considered only on the first part of the squeeze, from 11m down to 2m.

5.8c, a BP of duration of 595s seems reasonable. Shorter BPs with durations around 550s may also fit the requirements, however, the amount of time saved compared to the first one is not worth an increase of almost 1% of β_{beat}. There are large differences between BP with similar duration due to a different repartition of the same number of MP. The generation and simulation of all the BP possible to minimize the expected deviation would represent a significant amount of computing time. It is, however, possible to quickly converge to the minimum by starting with constant steps in β^* from initial to final value, and then vary slightly the size of the steps in order to have minimum step size where large deviations are expected.
Figures 5.9 shows the evolutions of the β^*s at IP8 and IP1, the latter being identical to the one in IP5, for the different BP generated during the optimisation procedure of the configuration of 2011. The longest BPs are clearly not optimized as there are significant time during which the β^* is not lowered at IP1 and 5. This time is wasted on waiting on IP8 which is lowered in a slower manner. Therefore most of the time is saved by removing extra intermediate steps in IP8, in order to lower the β^* synchronously during the first part. Another approach would be to squeeze IP8 asynchronously with regards to the other IPs such that the β^* is varied almost uniformly from initial to final value for all IPs. However, the aperture available in the triplets is shrinking while lowering the β^*s, therefore it is more convenient to squeeze all IPs synchronously in order to keep only two IPs at lower β^*, therefore minimizing the source of error when the machine is more sensitive to any beam disturbance.
It is relevant to note on figure 5.8c that the maximum deviation of beam parameters, and in particular β_{beat}, is dominated by the last steps. In particular, the step from $\beta^* = 1.5$m to 1.1m generated a critical $\beta_{\text{beat}}$for beam 2, especially in the vertical plane. The cause of this anomaly is not known, but further investigations and proper corrections are needed before squeezing down to these values. As no significant defect of both matched optics are revealed by the simulation, we can distinguish two cases. An error during the procedure to compute the matched optics has created this large β_{beat}in which case the problem may be corrected without having to add an intermediate step. Otherwise, the introduction of an additional MP will not change the results of the analysis presented.

5.4.4 Stopping points

As can be seen on 5.6, removing the possibility to stop at the MP may be beneficial in certain cases only. Indeed, in this example, the first non stopping MP do not allow to shorten the BP. When changing sign of the ramp rate, the derivative has to be null at a certain point, therefore fulfilling the same condition as a

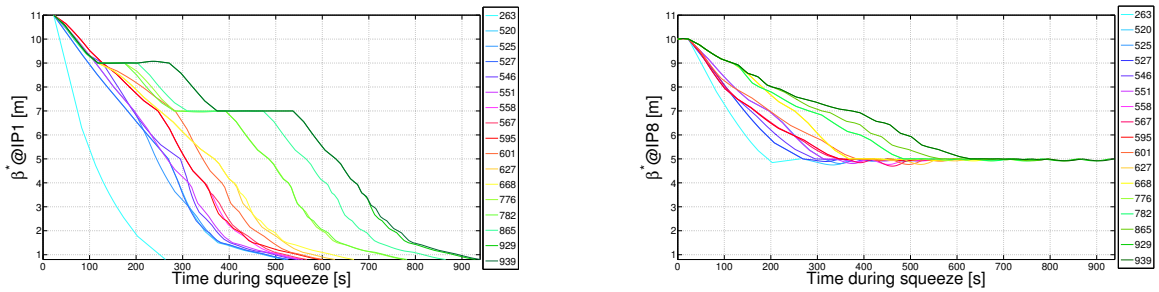

(a) IP1 (b) IP8

Figure 5.9: β^* for the different squeeze strategies.

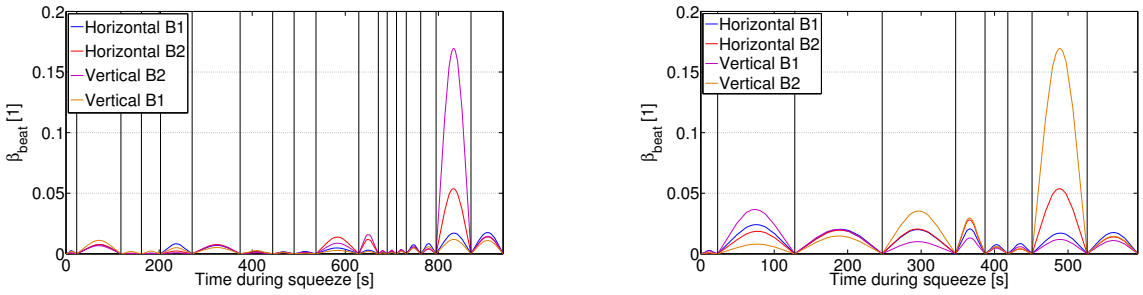

(a) Long (b) Optimised

Figure 5.10: Simulation of β_{beat}during the longest squeeze BP with $\beta^*_{\text{min}} = 0.8$m at IP1 and IP5 and $\beta^*_{\text{min}} = 5$m at IP8 i.e. all optics available have been used compared to the optimised one.

t [s]	β^* [m] IP1& 5	IP8
0	11	10
23	11	10
118	9	9
162	9	8.5
203	9	8
271	9	7.5
374	7	7
444	7	6.5
490	7	6
537	7	5.5

t [s]	β^* [m] IP1&5	IP8
629	5	5
671	4	5
690	3.5	5
710	3	5
731	2.5	5
762	2	5
795	1.5	5
870	1.1	5
939	0.8	5

(a) Long

t [s]	β^* [m] IP1&5	IP8
0	11	10
23	11	10
128	9	7.5
247	7	6
347	4	5
387	3	5
418	2	5
451	1.5	5
526	1.1	5
595	0.8	5

(b) Optimised

Table 5.2: Optic sequence of the longest and the optimised BP for 2011.

	IP1	IP2	IP5	IP8
Minimum β^* [m]	1.5	10	1.5	5

Maximum deviation	Horizontal		Vertical	
to nominal value	B1	B2	B1	B2
Tune [10^{-3}]	4.5	9.0	4.5	6.7
Chromaticity	0.2	0.2	0.3	0.3
β_{beat}[%]	2.4	2.8	3.7	3.5

Table 5.3: Minimum β^* and maximum deviation that can be expected based on the simulation for the BP proposed for operation in 2011.

stopping MP. However the benefit is clear in the second case, when the ramp rate do not change sign.
The minimum time is limited by the slowest magnet, therefore the minimum duration of each interval between two matched point has to be computed for all parameters, the settings of each has then to be adapted to the longest one. The computation of the minimum time for one setting is fairly simple, indeed, the minimum time is given by the time to go from the initial value to the final one with the maximum ramp rates in cases no changes of derivative is necessary and add the necessary time for the parabolic round off otherwise. Introducing the maximum ramp rate and acceleration I'_{max} and I''_{max}, the minimum time to change from I_i to I_f is Δt.

$$\Delta t = \begin{cases} \dfrac{|I_f - I_i|}{I'_{max}} & \text{No round off} \\ \dfrac{|I_f - I_i|}{I'_{max}} + n\dfrac{I'_{max}}{2I''_{max}} & n = 1, 2 \text{ round off} \end{cases} \tag{5.4.1}$$

Then the interval duration is ΔT.

$$\Delta T = \max_{parameter} \Delta t \tag{5.4.2}$$

The settings of the parameters have to be adapted to the limiting one, by introducing a slower ramp rate and accelerating from the previous ramp rate to the following at each MP with a parabolic round off. It is important to note that whereas the computation of the settings in between two MPs is completely decoupled from the other MPs when dealing with stopping MP, the non stopping point approach leads to a set of coupled equation that needs to be solved for each parameter. However, this computation is done on rare occasions, during the generation of the BP, the speed of the operation is therefore not relevant up to a reasonable limit.

Given the amount of parameters and the complexity of their specificities, the implementation of this method is not trivial and it is still a work in progress. The amount of time that can be saved will vary depending on which parameters vary in the slowest manner, therefore limiting the duration of the BP. Indeed, if the current in the limiting magnets follow monotone functions, the minimum time of the BP is the one that is needed for these magnets to ramp with maximum rate from initial value to the final one, which represents a gain of 60% to 70% depending on the BP. On the other hand, if the slow magnets are often changing ramp rate sign, the amount of time saved may be close to null. Only the implementation of the algorithm to compute the minimum time will give an accurate value.

5.4.5 Proposal for 2011

At first, it is important to note that because of the recent correction of a bug in the current generation algorithm, the duration of the squeeze will be diminished by 20% to 30% compared to the duration presented here even before applying any optimisation.
Secondly, the removal of appropriate MPs have shown to provide a reduction of the duration in the order of 20% to 30%, without expecting β_{beat}over 3.7% due to the unmatched optics. In particular, the optimised BP defined by the β^* configuration showed on table 5.2, allow to achieve the performances summarised in table 5.3 in 451s. Comparing the β^* sequence for the longer BP, we observe that much time has been saved by removing intermediate steps at the beginning of the squeeze, that is to say when the $\beta^* > 4$m. Most of the steps are kept when lowering the β^*s further. This approach allow to obtain maximum gain when the machine is the less critical.
In order to allow a fast commissioning of the squeeze, both the long and the optimised BPs will be prepared for operation. The long BP is kept as a fall-back in case significant troubles are encountered during the commissioning of the optimised solution.

5.4.6 Outlook

The potential of the non-stopping MP approach is not yet known, early results of an ongoing study suggest that the duration may be reduced by $\sim 20\%$ by transforming all intermediate MPs into non-stopping MPs. Keeping in mind that a non negligible number of stopping MPs are necessary during the commissioning phase, the efficiency of the optimisation is reduced and may not be worth implementing. Indeed, based on the timing study of the squeeze during the commissioning (fig. 4.9b), even though the possibility to stop is not used often, each of the MP is used at least once. Two approaches are worth further investigation. First, the need for MPs during the commissioning phase could be overcome by decoupling it from the standard operation. This could be achieved by introducing two different BP with an identical sequence of optic. One contains stopping MPs and is used for the commissioning. The correction applied are then adapted to the second that contains non stopping MPs. Second, an optimised beam process containing both stopping and non-stopping MPs can be worked out in order to obtain similar duration as the one already achieved by removing MP, except with improved β_{beat}.

5.4.7 Concurrent approaches

Combining ramp and squeeze The possibility to perform ramp and squeeze at the same time is considered as it would significantly reduce the turn around time. Indeed, the ramp rate during the ramp is limited by the main dipoles, therefore there exists a margin in which the strength of the quadrupole can be varied while ramping. This approach also has the advantage of dealing with exclusively up ramping magnets, therefore removing hysteresis related issues. This strategy has been kept aside in order to avoid having to commission two systems at the same time, which would have significantly increased the difficulty to both protect and understand the machine. In case ramp and squeezed are combined, minor adjustments to the tools developed for the previous analysis will be needed to allow a similar optimisation of the duration of the combination. It is however very likely that the overall time limit of the combination is not the ramp rate of the quadrupoles but the one of the dipoles. In this case, the minimum duration of the combination is the current duration of the ramp, that is to say the time saved is the current duration of the squeeze, which is in the order of 20 minutes.

Luminosity levelling In order to maximise the integrated luminosity, a levelling of the luminosity may be introduced. Luminosity levelling consist of diminishing the peak luminosity to the advantage of a longer beam lifetime. This can be done by varying the β^* while beams are colliding. This study case is completely different from the one presented in this thesis, as the dominant effect is beam-beam interaction. Several approaches are being considered to implement a luminosity levelling, however a further understanding of the behaviour of the machine while colliding higher intensity beams is needed to find the most appropriate one. No levelling is therefore expected in a near future. Moreover, among the luminosity levelling strategies, the variation of β^* is disfavoured by the observations made on the Tevatron at Fermilab.

Chapter 6

Conclusion

The performance of the LHC in 2010 regarding the squeeze is excellent. Most importantly, the amount of beam lost during this operation is lesser than one percent and the fill to fill reproducibility of the beam parameters is remarkable. This finding allow to approach the optimisation of the squeeze in different aspects. Firstly it has been shown that advantage can be taken from the good reproducibility to lessen the dependency on the feedback system availability and to better correct parameters that are not controlled by feedback systems by introducing a correction based on measurements performed during the previous fills. The long term stability of each parameter do not justify the introduction of an automatic feed-forward system, however the basis of an application that, among other purposes, aims to facilitate the manual feed-forward has been developed and is planned to be provided to the operator before the restart in 2011.
Secondly, a study of some systematics, notably regarding the losses, have allowed to point out issues that will be corrected for next year. Most importantly, the comparison of simulation and measurement of the tune as well as considerations on orbit measurements have allowed to point out that hysteresis of the quadrupole is not handle properly. It is suggested that the hysteresis of the magnet will have a lower impact on the beam dynamics than the effects of the current treatment.
The potential of the analysis of systematics has not been fully harnessed yet, further studies are still on going. In particular, such studies may be extended to other BPs such as the energy ramp.

Event though the duration of the squeeze is not currently the primary concern regarding the turnaround time, it will become relevant when other longer operations are fully optimised. For example, the turnaround time is currently dominated by the injection which duration is significantly longer than the nominal one. In this line of thought the duration of the squeeze is minimized based on simulation of the beam parameters during the change of optics performed during the squeeze. It has been shown that reduction of 20% to 30% of the duration may be achieve using the implementation already available without expecting too large deviation of the beam parameters with regards to their nominal value caused my the mismatching of the settings. In particular, a new configuration is proposed for standard operation in 2011, which will be used as a baseline for the commissioning.
A new perspective was also proposed that would allow to gain a significant amount of time. This method however requires a significant amount of work for its implementation and the amount of time saved is still uncertain. A draft of the new algorithm is presented in appendix A, its implementation may be tested during the year during non-standard operation. The benefits of this method needs to be compared with more challenging but also more interesting methods to reduce the time dedicated to the squeeze.

Bibliography

[1] ATLAS Collaboration, "Atlas detector and physics performance," Technical Design Report, CERN, Geneva, Switzerland, May 1999.

[2] CMS Collaboration, "Cms physics," Technical Design Report, CERN, Geneva, Switzerland, June 2006.

[3] LHCb Collaboration, "Lhcb reoptimized detector design and performance," Technical Design Report, CERN, Geneva, Switzerland, September 2003.

[4] ALICE Collaboration, "Alice physics performance report," CERN, Geneva, Switzerland, December 2005.

[5] A. Valishev, G. Annala, D. Bollinger, B.Hanna, A. Jansson, T. Johnson, R. Moore, D. Still, C.-Y. Tan, and X. Zhang, "Recent tevatron operational experience," in *Proceedings of PAC09*, (Vancouver, Canada), 2009.

[6] S. Lee, *Accelerator Physics*. World Scientific Publising Co. Pte. Ltd., 2004.

[7] Y. Luo, P. Cameron, S. Peggs, and D. Trbojevic, "Possible phase loop for the global betatron decoupling," *BNL - C- A/AP*, October 2004.

[8] "Lhc design report," CERN, Geneva, Switzerland, 2004.

[9] R. Steinhagen, "Performance and lhc beam stability issues related to q/q' diagnostics and feedback systems," in *Proceedings of the 2010 Evian workshop on LHC commissioning*, (Evian, France), 2010.

[10] N. J. Sammut, *The Field Description for The Large Hadron Collider*. PhD thesis, University of Malta, July 2006.

[11] M. Aleksa, S. Russenschuck, and C. Völlinger, "Magnetic field calculations including the impact of persistent currents in superconducting filaments," *IEEE Transactions On Magnetics*, vol. 38, Mar. 2002.

[12] M. Gasior, A. Boccardi, R. Jones, and R. J. Steinhagen, "An overview of the lhc transverse diagnostics systems," LHC Project Report 1166, CERN, Geneva, Switzerland, Mars 2008.

[13] D. Belohrad, J.-J. Gras, L. K. Jensen, O. R. Jones, M. Ludwig, P. Odier, J. J. Savioz, and S. Thoulet, "Commissioning and first performance of the lhc beam current measurement systems," in *Proceedings of IPAC'10*, (Kyoto, Japan), 2010.

[14] G. Kruk, S. Deghaye, M. Lamont, M. Misiowiec, and W. Sliwinski, "Lhc software architecture [lsa] - evolution toward lhc beam commissioning," in *Proceedings of ICALEPCS 07*, (Knoxville,USA), 2007.

[15] M. Allitt, A. S. Badal, C. Giloux, M. Karppinen, A. Lombardi, V. Remondino, W. V. Delsolaro, and R. Wolf, "Field quality and hysteresis of lhc superconducting corrector magnets," in *Proceedings of EPAC04*, (Lucerne, Switzerland), 2004.

[16] R. Tomas, O. Bruning, M. Giovannozzi, P. Hagen, M. Lamont, F. Schmidt, and G. Vanbavinckhove, "Cern large hadron collider optics model, measurements, and corrections," *Physical Review Special Topics - Accelerators And Beams*, 2010.

[17] CERN, *http://mad.web.cern.ch/mad/*.

[18] R. J. Steinhagen, A. Boccardi, E. C. Giraldo, M. Gasior, J. L. Gonzalez, and O. R. Jones, "Continuous measurement and control of beta-beating in the lhc," in *Proceedings of IPAC'10*, (Kyoto, Japan), 2010.

[19] C. A. Pons, X. Buffat, M. Giovannozzi, G. Müller, S. Redaelli, K. Fuchsberger, M. Lamont, and F. Schmidt, "The online model for the large hadron collider," in *Proceedings of IPAC'10*, (Kyoto, Japan), 2010.

Appendix A

Generation algorithm

The algorithm presented here is an intermediate draft of a work in progress. It shows the leads that are followed in order to implement the non stopping point approach in the control system of the LHC.
The new algorithm to generate the settings of the parameter during the squeeze BP is more complicated than the current one as each interval between two MPs can no longer be considered independently. Indeed, according to figure A.1, the derivative of the $n-1$ interval between the n non stopping MPs and the two interval between the stopping MPs with the others are all linked together. In order to compute properly the settings of each parameter in an optimized way, I propose an algorithm in two distinct parts. First, the time of each MP $t_0, ..., t_{n+1}$ is computed taking into account the limitations of each magnet. In a second part, each settings is computed in between the MPs.

A.1 Computing the times

The times of the MPs is limited by the slowest magnet, which may different for each interval. Therefore, the shortest duration of each interval may be computed for each parameter taking into account the proper limitation. Then, the duration of the interval is set to the longest one among all parameters. Then the times may be computed as follow iteratively from $T_0 = 0$, introducing the ensemble of all parameters $\mathcal{P}$

$$t_{i+1} = t_i + \max_{p \in \mathcal{P}} (t(p)_{i+1} - t(p)_i) \tag{A.1.1}$$

As discussed previously, certain parameter follows monotone functions whereas others follow more complicated ones. It as been seen that no advantage is expected in case of a change of sign of the derivative, as the derivative at the MP is zero anyway. Therefore the computation can be done by considering the BP as a sequence of monotone part. It is important to note that the sequence is different for each parameter, as the change of sign of the derivative occur at different MPs. For the validity of the algorithm, it is also necessary to consider the passage from non null to null value as a change of sign of the derivative. Let us consider a sub part of the BP as shown on figure A.1 assuming that the setting of the parameter considered is monotone from T_0 to T_{n+1}. Two cases needs two be considered, whether there is non stopping MPs or not. In case

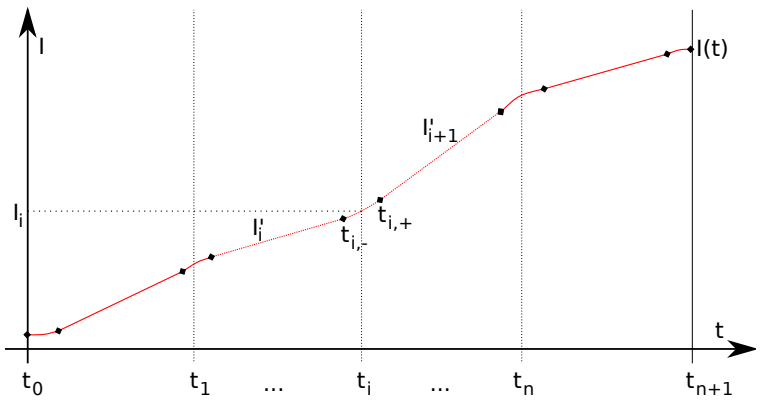

Figure A.1: Definition of the beam process to study.

there is no non stopping MP, i.e $n = 0$, the minimum time is given by :

$$\min(t_{i+1} - t_i) = \begin{cases} 2\sqrt{\dfrac{I_{i+1} - I_i}{I''_{\max}}} & , \sqrt{I''_{\max}(I_{i+1} - I_i)} \leq I'_{\max} \\ \dfrac{|I_{i+1} - I_i|}{I'_{\max}} + \dfrac{I'_{\max}}{2I''_{\max}} & , \text{otherwise} \end{cases} \tag{A.1.2}$$

This case corresponds to the current algorithm of generation and will therefore not be discussed further. In case $n \geq 1$, the minimum time is given by ramping straight from one value to another with the maximum ramp rate in between the non stopping MP, and adding the time for the necessary parabolic round off at the beginning and at the end.

$$\min(t_{i+1} - t_i) = \begin{cases} \dfrac{|I_{i+1} - I_i|}{I'_{\max}} & , i = 1, ..., n-1 \\ \dfrac{|I_{i+1} - I_i|}{I'_{\max}} + \dfrac{I'_{\max}}{2I''_{\max}} & , i = 0, n \end{cases} \tag{A.1.3}$$

A.2 Generating the settings

In order to compute the derivative in the interval between the MPs, the equation of each transition may be put together in order to obtain a system of equation. The current around the non stopping MP is :

$$J_i(t) = \begin{cases} b_{i,0} + I'_i(t - t_i) & t < t_{i,-} \\ a_{i,0} + a_{i,1}t + a_{i,2}t^2 & t_{i,-} \leq t \leq t_{i,+} \\ c_{i,0} + I'_{i+1}(t - t_i) & t > t_{i,+} \end{cases} \tag{A.2.1}$$

Introducing the condition of continuity of the function and the derivative as well as the value of the parameter at the MP for each J_i, for clarity the index i has been dropped. Moreover, we impose that the acceleration is always the maximum one.

$$\begin{cases} J(t_-) & = a_0 + a_1 t_- + a_2 t_-^2 & = b_0 + I'_i(t_- - t_i) \\ J(t_+) & = a_0 + a_1 t_+ + a_2 t_+^2 & = c_0 + I'_{i+1}(t_- - t_i) \\ \frac{dJ}{dt}(t_-) & = a_1 + 2a_2 t_- & = I'_i \\ \frac{dJ}{dt}(t_+) & = a_1 + 2a_2 t_+ & = I'_{i+1} \\ J(t_i) & = a_0 + a_1 t_i + a_2 t_i^2 & = I_i \\ \frac{d^2J}{dt^2}(t_i) & = 2a_2 & = \pm I''_{\max} \end{cases} \tag{A.2.2}$$

Considering this set of equation for each MP give rise to an under constrained non linear system, a solution of which could be found using numerical algorithm. However, such approach is disfavoured at this level of the implementation, as high precision and robustness is required. Workarounds are under study to properly solve this system in an analytical way.

Appendix B

Java application

B.1 Beam process scanner

The Online Model [19] is an application that aims to provide MADX simulation in the control room of the LHC. The simulation of BP presented in chapter 5 are performed within the Online Model. A new package, *cern.accsoft.om.app.bpscan*, has been developped in order to perform the simulation using the tools provided by the Online Model and JMad, a java application programming interface for MADX simulation. As a part of the Online Model, the basic features of the package are accessible from the control room via a simple panel shown on figure B.1. The panel offers the possibility to plot beam parameters listed below as a function of time during the BP studied. The possibility to make 2D parametric plots of a beam parameter as a function of another is also available.

Global

1. Tune
2. Tune split
3. Chromaticity
4. β_{beat}

Local

1. Orbit
2. β
3. Multipolar magnetic strength

The local parameters are computed at a position defined by either the s coordinate or the name of the object defined by the MADX sequence file.
The manipulation of settings such as the introduction of the fake changes of hysteresis branch are not available through the graphical user interface. However, if such a graphical interface turns out to be useful, the development needed to introduce it is quite small.

B.2 Data mining

In order to efficiently perform analysis of measurements during a BP, fast access to the settings of the machine and the measurements as a function of time is needed. These informations are stored in two distinct databases, LSA and logging respectively, that rely on fundamentally different implementations. Even though the graphical user interfaces provided are powerful tools for data mining, especially in the context of the control room, the differences in implementation is often limiting the efficiency. In that state of mind, a new package was developed in order to fill the needs to the study presented in this thesis. Its main advantage is to encapsulate both databases in a consistent way, such that informations of both databases can be handled easily. The resulting application may serve for the purposes of other study. For example, the studies performed here may prove to be useful while pushing the performances of the LHC. Based on the experience acquired during 2010, notably concerning the advantage of a feed forward approach, an application with graphical interface may be produced for the beginning of next run mainly providing the features listed below for the operators.

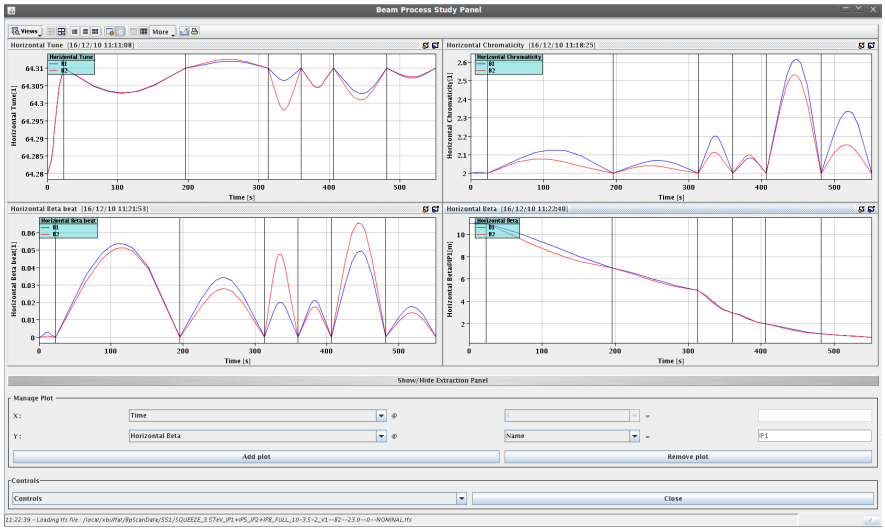

Figure B.1: The graphical user interface of the beam process scanner.

1. Statistical analysis of beam parameters during a BP over selected fills.
2. Automatic selection of fills of interest for the statistics based on a list of criterion.
3. Automatic check of PC synchronisation based on the measurement of the current in each PC.